CTU

CZECH TECHNICAL UNIVERSITY IN PRAGUE

Faculty of Electrical Engineering

Department of Control Engineering

Master's thesis

Atmospheric water generator optimization

Bc. Pavel Souček

2022

Supervisor: Ing. Jiří Dostál

MASTER'S THESIS ASSIGNMENT

I. Personal and study details

Student's name: **Souček Pavel** Personal ID number: **466376**

Faculty / Institute: **Faculty of Electrical Engineering**

Department / Institute: **Department of Control Engineering**

Study program: **Cybernetics and Robotics**

Branch of study: **Cybernetics and Robotics**

II. Master's thesis details

Master's thesis title in English:

Atmospheric water generator optimization

Master's thesis title in Czech:

Optimalizace zařízení pro získávání vody ze vzduchu

Guidelines:

1) study AWG devices, dynamical model calibration and optimization
2) create a mathematical model of AWG
3) calibrate the mathematical model
4) construct an AWG production optimization problem

Bibliography / sources:

[1] Boyd, S., & Vandenberghe, L. (2004). Convex Optimization. Cambridge: Cambridge University Press. https://doi.org/10.1017/CBO9780511804441
[2] Rang Tu, Yunho Hwang, Reviews of atmospheric water harvesting technologies, Energy, 201, 2020, https://doi.org/10.1016/j.energy.2020.117630.

Name and workplace of master's thesis supervisor:

Ing. Jiří Dostál Department of Control Engineering FEE

Name and workplace of second master's thesis supervisor or consultant:

Date of master's thesis assignment: **15.02.2022** Deadline for master's thesis submission: **20.05.2022**

Assignment valid until: **19.02.2024**

Ing. Jiří Dostál	prof. Ing. Michael Šebek, DrSc.	prof. Mgr. Petr Páta, Ph.D.
Supervisor's signature	Head of department's signature	Dean's signature

III. Assignment receipt

The student acknowledges that the master's thesis is an individual work. The student must produce his thesis without the assistance of others, with the exception of provided consultations. Within the master's thesis, the author must state the names of consultants and include a list of references.

.	
Date of assignment receipt	Student's signature

Declaration

I declare that the presented work was developed independently and that I have listed all sources of the information used within it in accordance with the methodical instructions for observing the ethical principles in the preparation of university theses.

In Prague, 19. May 2022

. . . . . .

Pavel Souček

Acknowledgement

I would like to thank my supervisor Ing. Jiří Dostál for assigning me this particular thesis and providing me with regular meaningful consultations. I also must not forget to express my gratitude to my family, who supported me during my studies and in my life in general.

Abstract

This thesis investigates the topic of generating water from the air. In particular, a control optimization of one exact realization of an air-water-generator (AWG) called AWG-DW, where DW stands for desiccant wheel. The main goal of the thesis is to model, calibrate and control AWG-DW such that the production of water is maximized. First, models of the individual AWG-DW components are created and validated by available measured data. Despite some inconsistencies in the provided data, the best possible complete model of AWG-DW was derived. Possible explanations for the errors were proposed, however, further investigation is needed. The component and system constraints were added to complete the system description. The water production maximization task was broken down into three parts - finding a steady state operating point and setpoint optimization for on-grid and off-grid conditions. The results show that for an off-grid operation the device is most efficient (production per watt) when the electric heater is not in use. The overall limiting factor is often the freeze build-up prevention on the evaporator or the maximal refrigerant pressure in the condenser. For on-grid usage, the heater is activated up to the limit of the desiccant wheel upper temperature constraint for maximum water production per hour.

Keywords: Air water generator, AWG, static optimization, steady state, nonlinear system, automatic differentiation, heat exchanger, desiccant wheel, dehumidification, nonlinear optimization

Abstrakt

Tato diplomová práce se zabývá tématem generování vody ze vzduchu. Především na optimalizaci jednoho takové zařízení za získávání vody ze vzduchu zvané AWG-DW. Hlavním cílem této práce je modelovat, kalibrovat řídit toto zařízení na generování vody tak, aby byla maximalizována produkce vody. Nejprve jsme vytvořili modely jednotlivých komponent zařízení a porovnali jejich výsledky s naměřenými daty. I přes problémy nalezené v naměřených datech jsme vytvořili nejlepší možný model. Možná vysvětlení nekonzistence dat byla navržena, ale bez dalšího měření nebylo možné jednoznačně určit příčinu. Popis systému jsme doplnili o limity jednotlivých komponent. Optimalizační úloha byla rozdělena na tři částí – hledání ustálených stavů a hledání optimální setpointů pro maximalizaci produkce vody při připojení přístroje ke zdroji omezenému nebo neomezenému elektřiny. Výsledky ukázaly, že pokud je zdroj elektřiny omezený, tak zařízení je nejúčinnější (produkce vody na elektrický příkon), pokud elektrický ohřívač není používat a hlavním omezujícím faktorem je prevence namrzaní výparníku nebo maximální tlak chladiva v kondenzátoru. Pokud je zařízení připojeno k neomezenému zdroji elektřiny, tak je elektrický ohřívač používán, dokud není dosažena maximální teplota desikačního kola.

Klíčová slova: Generování vody ze vzduchu, statická optimalizace, ustálené stavy, nelineární systémy, automatická diferenciace, teplotní výměník, desikační kolo, odvlhčování, nelineární optimalizace

Contents

List of Figures

List of Tables

Chapter 1
Introduction

Worldwide, many different ways to harvest water are utilized. Rainwater can be collected, seawater can be desalinated or groundwater can be harvested. However, if there are none of those liquid water sources, then the harvesting of the atmospheric water is an option. This is especially true in the deserts, where the water is scarce.

Many researchers (e.g., [1, 2]) have already reviewed this topic of water harvesting. There are at least three ways used to harvest water from the air. First of them is a fog collection, where the water droplets are trapped by a mesh and the water is then accumulated in a collector. The main disadvantage of this approach is that in regions where the water is scarce the fogs tend to be rare as well.

The second technology is the harvesting of water using condensation. In this approach, air flows along a surface whose temperature is lower than the dew temperature of the air. Therefore the water moisture condensates at the surface. These technologies require electricity as active cooling is needed. Vapor compression cycle or Peltier effect are often utilized as a cooling source.

The third approach is sorption technology which catches moisture at night when the humidity is higher with adsorbent or absorbent. Those technologies tend to have lower daily water harvesting capacity compared to other technologies.

Atmospheric water harvesting devices can consist of many internal parts. The individual component dynamics influence each other, therefore, the behavior of such devices can be complex. Understanding the working principle as well as determining the optimal operating conditions for such devices can get complicated.

This thesis aims to develop a model of the steady-state behavior of an air water generator (AWG) and utilize it for optimization of one of such devices based on [3, 4]. For the purpose of this thesis, we will call this device AWG-DW as it utilizes the desiccant wheel to increase its water production in the arid environment in countries such as Saudi Arabia.

There are four main objectives for this project. Three of them were accomplished as a part of this thesis and the fourth one is a topic for further research. Firstly, we wanted to create a model which can calculate an expected water generation rate. In this model, we want to find the optimal internal setpoints which will achieve the best water production rate given the outside air temperature, humidity, and total input power of the device. We also set a constant airflow rate through the evaporator. The reason for the constant flow rate is that almost all measurements were measured with this constant flow rate and we are concerned with the accuracy of the model at different evaporator air flow rates.

Secondly we will investigate the case when the input power is abundant, for example, when the device is powered from the electric grid. In this scenario, we want to maximize the water production.

Thirdly, we want to investigate the case when the input power is limited, for example, when batteries power the device. Therefore, we will use the model of the device to find the most efficient internal setpoint i.e. where the water production is highest per unit of input power. Once again, at the constant evaporator air flow rate.

Lastly, AWG-DW was built to be powered by a combination of solar panels and batteries. Therefore, we plan to create an economic model predictive controller to maximize production throughout the day. However, we will not cover this topic in this thesis.

1.1 The basic operating principle of the device

AWG-DW was engineered to operate in places with very low air humidity. Therefore, a great effort was put into increasing absolute air humidity. The schematic of this device is in schematic 1. First, the air is pushed by the fan ‘F1’ and preheated by the sub-cooler ‘SC’ and the condenser ‘C’ of the heat pump. It is then heated even more by the electric heater ‘H’. In the desiccant wheel ‘DW’, the air is cooled and its water content is increased. The desiccant wheel dynamics are complex, however, with some simplification, we can say that the higher the temperature difference between the temperature of the air coming into the desiccant wheel from the electric heater and the outside air, the bigger is the increase in the air absolute humidity. We describe the mechanism of heat and mass transfer in the desiccant wheel in Section 2.9.

The moist air from the desiccant wheel is then fed through one side of the recuperator ‘RC’, where it is cooled. The water from the moist air is then condensed in the evaporator ‘E’. The cold air from the evaporator is reused in the second side of the recuperator. There it heats up in order to cool the air coming from the desiccant wheel.

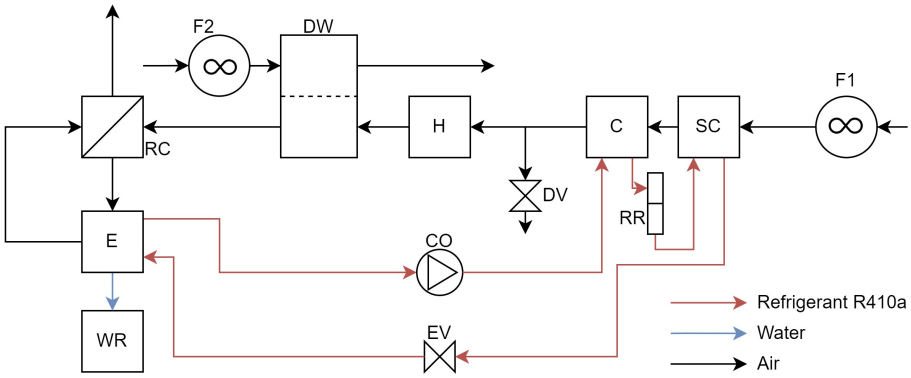

Figure 1: Schematic of AWG-DW device

C	condenser	SC	sub-cooler
EV	expansion valve	CO	compressor
RR	refrigerant receiver	E	evaporator
H	electric heater	DV	dumper air valve
DW	desiccant wheel	RC	recuperator
F1	regeneration air fan	F2	process air fan
WR	distilled water reservoir		

There is also a dumper air valve ‘DV’. This valve is used when an increase in the heat transfer in the condenser and the sub-cooler is needed, thus decreasing the condensation temperature of the heat pump and increasing its cooling capability.

The second fan ‘F2’ pushes the outside air through the second side of the desiccant wheel. This air is the second medium of heat and mass transfer in the desiccant wheel. While flowing through the desiccant wheel, the air from the second fan gains heat and transfers the moisture through the wheel into the air on the other side.

1.2 Moist air fundamentals

In general, the moist air may contain a variable amount of water vapor from zero (dry air) up to the maximum it can contain (saturated moist air). In this chapter, we describe basic relations regarding the properties of moist air. The absolute humidity (also called humidity ratio) X is defined as the mass of water vapor m_w divided by the mass of moist air $m_{a,dry}$.

$$X = \frac{m_w}{m_{a,dry}} \tag{1}$$

Relative humidity is another way to describe the amount of water in the air as the ratio of the partial pressure of the water vapor p_v and the saturated water vapor pressure at a given temperature $p_{vs}(T)$

$$\mathrm{RH} = \frac{p_v}{p_{vs}(T)}. \tag{2}$$

Water content in the air can be expressed by the pressure of the air P_a and the partial pressure of water vapor p_v

$$X = 0.62198 \frac{p_v}{p_a - p_v}. \tag{3}$$

As an approximation of the saturated vapor pressure ($p_{vs}(T)$) we used the Tetens equation 4. However, there are many other possible approximations.

$$p_{vs}(T) = 610.78 e^{\frac{17.27\ T}{T+237.3}} \tag{4}$$

Expression describing humidity ratio of air as a function of temperature and relative humidity can be obtained by combining equations Eqs. (2) to (4)

$$X = \frac{3.799\,\mathrm{RH}\,\mathrm{e}^{\frac{17.27\,T}{T+237.3}}}{p_a - 6.108\,\mathrm{RH}\,\mathrm{e}^{\frac{17.27\,T}{T+237.3}}} \tag{5}$$

When the air temperature decreases, the ability to store water is reduced as well. Dew temperature is the temperature at which the air is saturated, i. e., has 100 % relative humidity. If the temperature of some surfaces is below the dew temperature, then the water from the air will condensate at this surface. The dry bulb temperature is the temperature that a regular sensor measures when placed into the measured air. The Psychometric chart (Fig. 2) visualizes Eqs. (1) to (5) of the temperature, relative humidity and absolute humidity.

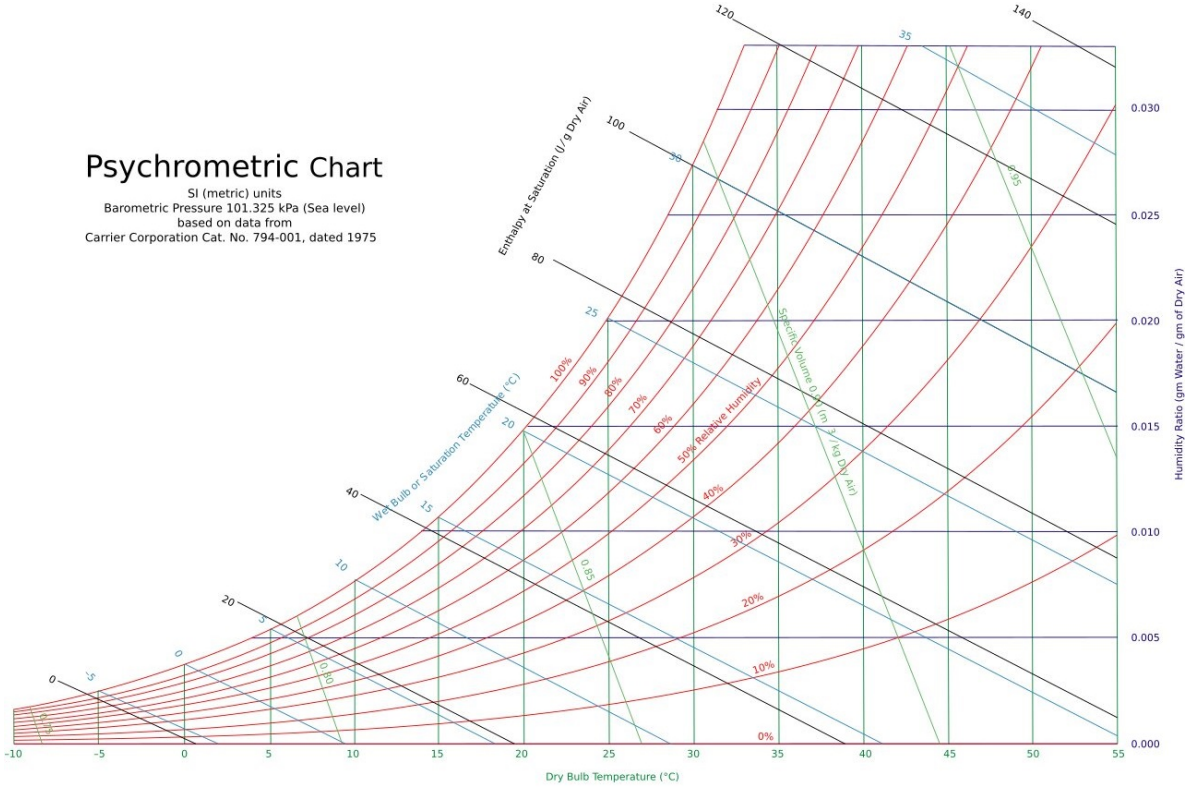

Figure 2: Psychometric chart [1]

[1] https://isaacscienceblog.com/2017/11/20/psychrometric-charts

1.3 Refrigerant cycle

A refrigerant cycle, also called the vapor compression cycle, is a thermodynamic cycle that transfers heat from one medium to another. It can be utilized for both heating and cooling. The refrigerant cycle takes advantage of the relation between the pressure and the refrigerant's saturation (boiling) temperature. The refrigerant is pressurized and condensed transferring its latent heat in the process. The pressure is then lowered to reduce the saturation temperature so it can evaporate once again. After that, the compressor increases the pressure of the gas and the cycle repeats. This way, the refrigerant can gain thermal energy in the form of latent heat of evaporation at a place with a low temperature and then transfer it to a place with a higher temperature.

The saturation line of the refrigerant in the pressure-enthalpy diagram is shown in Fig. 3 beside the refrigeration cycle marked with the numbers 1 to 4. Under the saturation line, the refrigerant is a mixture of gas and liquid. The left part of the saturation line is the liquid saturation line, where the refrigerant is fully liquid. The right part of the saturation line is the gas saturation line, where the refrigerant is entirely gaseous. The critical point is on the top, where the liquid and gas lines meet. Above this point, the state transition between gas and liquid ceases to exist. The enthalpy difference between the gas saturation line and the liquid saturation line is the latent heat of vaporization for different pressures. The majority of heat transferred in a refrigerant cycle is the latent heat of evaporation. Therefore, it has a significant influence on the efficiency of the refrigerant cycle.

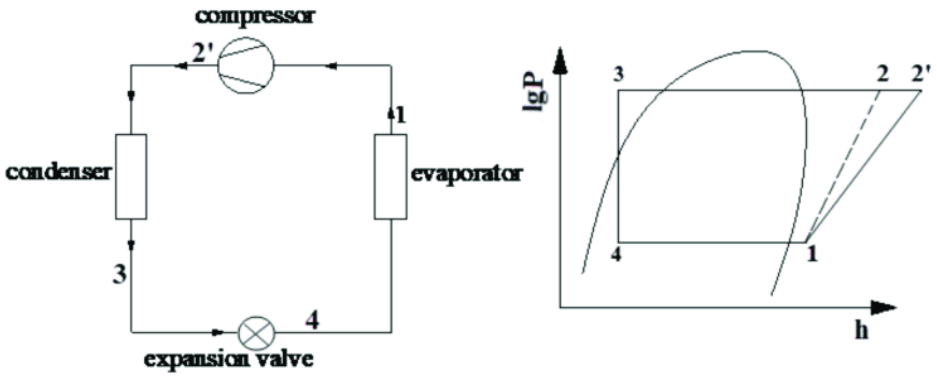

Figure 3: Diagram of heat pump working principle [5]

The refrigerant cycle can be found freezes, air conditioners and heat pumps. They are all the same in operational principle, but they differ in usage. Freezers and air conditioners are cold sources, while heat pumps are utilized as heat sources. In AWG-DW, the refrigerant cycle is both a heat source as well as a cold source. We decided to use the term heat pump for the description of AWG-DW. The heat pump consists of four major parts: condenser, expansion valve, evaporator and compressor.

A condenser is a heat exchanger that transfers heat between the refrigerant and the secondary medium, for example, air, water or earth. The refrigerant comes into the condenser as a super-heated vapor (point *2'* in Fig. 3) so its temperature decreases at first. When it reaches its saturation (condensation) temperature, it stays at this temperature until it becomes fully liquid. The refrigerant is then usually collected in a liquid receiver or at a lower place in the pipe. After that the refrigerant is sub-cooled (point *3*). During the sub-cooling, the refrigerant temperature lowers once again as the heat is transferred from the refrigerant. The heat pump in AWG-DW as well as in many other heat pump systems has a dedicated sub-cooler to increase the efficiency of the heat pump.

After the condenser, the refrigerant goes through the expansion valve (points *3-4*). The refrigerant's pressure decreases. Some amount of the refrigerant often evaporates during this process. The enthalpy of the refrigerant stays the same as there is no heat transfer and no work is being done during this process. In some heat pump systems, for example, in fridges, the expansion valve is just a small

pipe that has high resistance to limit the flow. In more complex systems, the valve is electronically controlled.

When the expansion valve is electronically controlled, it is usually done by a so-called super-heat controller. The job of this controller is to ensure that the refrigerant at the input of the compressor is a super-heated gas. If some refrigerant at the compressor input is still liquid, it usually results in damage to the compressor. If the gas is super-heated more than needed, it usually lowers the heat pump system's overall efficiency because the compressor's suction pressure is unnecessarily low.

The evaporator is the second heat exchanger in the heat pump (points *4-1*). However, due to the low pressure, the refrigerant evaporates even though its temperature in the evaporator is lower than in the condenser. The heat is transferred into the refrigerant, therefore, its enthalpy increases. If we neglect the pressure loss due to the friction of flow, then the process is considered isobaric.

The last major part of the heat pump system is the compressor (points *1-2'*). The pressure of the gas refrigerant is increased in this component. The compressor is doing work on the refrigerant, therefore, its enthalpy and temperature increase. Ideally, the process is adiabatic and isentropic, however, in reality, it is not due to various inefficiencies. The efficiency of the compressor is determined by

$$\eta_{ie} = \frac{\Delta H_{ie}}{\Delta H_{\text{actual}}} = \frac{H_2 - H_1}{H_{2'} - H_1}. \tag{6}$$

where ΔH_{die} is the discharge enthalpy change for the isentropic compression which denotes that the process is adiabatic, reversible and there is no entropy change and ΔH_{actual} is the real discharge enthalpy change. The isentropic compression as well as the actual are visible in chart 3 denoted as *2* and *2'* respectively.

The power of the compressor is determined by the enthalpy change and the mass flow

$$P = \dot{m}\Delta H_{\text{actual}} = \dot{m}\left(H_{2'} - H_1\right). \tag{7}$$

There are also other components of the heat pump system, for example, a 4-way valve, liquid separator, filter dryer and refrigerant accumulator. However, these devices do not influence the main working principle.

The efficiency of the heat pump is expressed by a coefficient of performance (COP) as the ratio of the heat transferred and input energy. The higher the value of COP, the more efficient the heat pump is

$$COP = \frac{Q}{W}. \tag{8}$$

The choice of the suitable refrigerant is determined by the saturation temperatures, which the heat pump system should achieve, as well as by the characteristics of the compressor and other equipment. Refrigerant R410a was used in AWG-DW. The pressure-enthalpy diagram is displayed in Fig. 4.

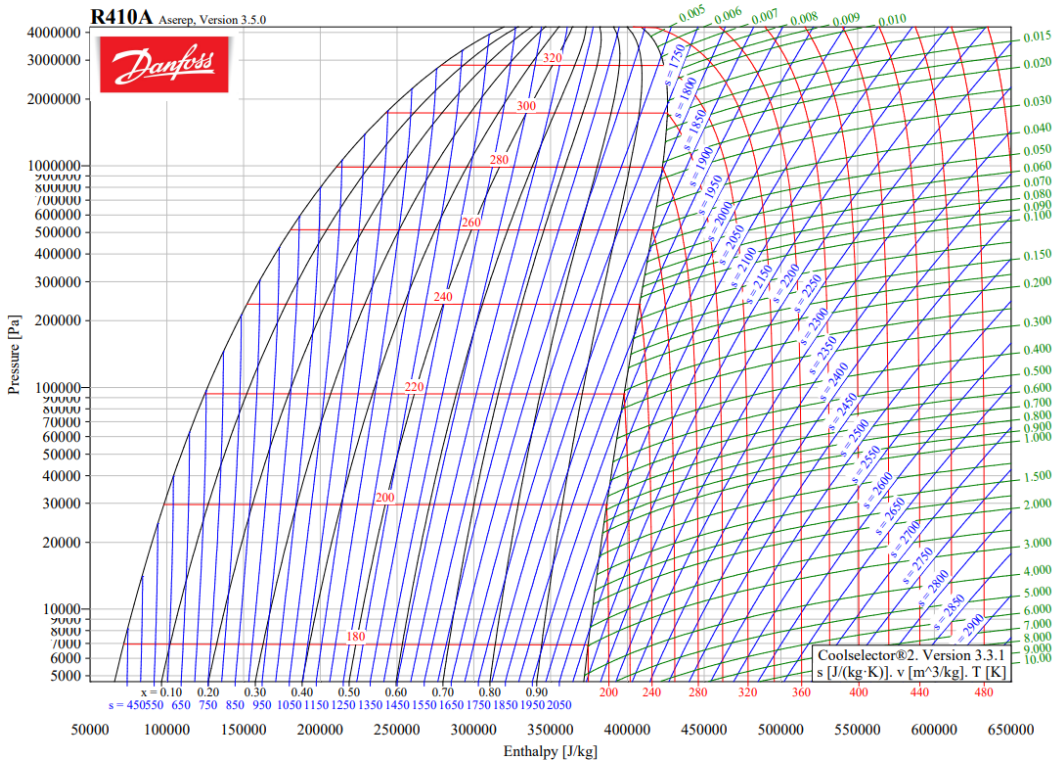

Figure 4: Pressure-enthalpy diagram for R410a [2]

[2] https://theengineeringmindset.com/r410a-pressure-enthalpy-chart

1.3.1 Heat pump inputs and modeling

If we consider the input airflow properties in the evaporator and the condenser to be constant, then by fixing two other properties of the heat pump system, we can determine all the variables. There are many options for how to choose those two variables. The natural choice would be the compressor's rotation speed and the expansion valve's position because these two values are controllable in a real heat pump system. Those two values together determine mass flow rate and the pressure in the evaporator as well as in the condenser.

Here we explain the main principles of the heat pump calculations which we utilize. Based on them, we can calculate the steady state of the heat pump system. The mass flow rate of the compressor is roughly linearly dependent on the rotation speed and the density at the suction port. The mass flow rate in the expansion valve is determined by the pressure difference. The liquid receiver between the condenser and sub-cooler collects the liquid refrigerant. This means that in the steady state, the condensation rate in the condenser has to be equal to the flow rate of the refrigerant. The saturation pressures in both heat exchangers determine the saturation temperature and the relation between the temperature and the enthalpy of the refrigerant. This relation between the enthalpy and temperature determines the heat exchange rate for a given refrigerant flow rate. With those principles in mind, we can build a model that can determine all the variables only from two variables.

However, if the compressor's speed and the expansion valve's position were chosen as our inputs of the heat pump (except the properties of air), it would not ensure many of the conditions required for the proper operation of the heat pump. In many heat pump systems, including the one in our AWD device, the expansion valve is controlled by the super-heat controller. Therefore, any combination of the compressor rotation speed and position of the expansion valve that does not satisfy the super-heat control algorithm does not give a valid result. We want to limit the saturation temperature in the evaporator to prevent the frosting of the evaporator. We also expect the optimal saturation temperature in the evaporator to be as low as possible.

For those reasons, we decided to use a different set of variables as our two degrees of freedom of the heat pump: the saturation temperature in the evaporator and the super-heat temperature. The super-heat temperature is the temperature difference between the saturation temperature and the temperature of the super-heated vapor at the compressor input. We implemented the super-heat controller as a part of the expansion valve. With this set of inputs, the refrigerant mass flow rate which achieves the predefined super-heat temperature can be calculated. In a steady state, the refrigerant condensation is equal to the flow rate in the condenser, therefore, the saturation pressure in the condenser is calculated to satisfy this condition.

The exact relations between all the variables in a heat pump system are more complex and its components influence each other in many intricate ways. For example, the pressure in the condenser is influenced by the compressor output enthalpy and which is determined, apart from other things, by the pressure in the condenser. Another example in AWG-DW is that the heat transfer in the condenser influences the air temperature at the evaporator's input. Each component is discussed in the appropriate subsection in more detail.

Chapter 2
Modeling of components

It would be extremely difficult to model the whole device. Therefore we decided to split it into its individual components, create models for them and then build the whole device from them.

Before the beginning of this thesis, 22 experiments were measured. The steady state values of those measurements can be found in appendix A. These values will be used in all models to evaluate the accuracy of our component models.

When modeling the components of AWG-DW, we could use one of three ways to describe their behavior. We can describe them as 'black boxes' using, for example, polynomial interpolation or neural network. This way, we can theoretically achieve the best accuracy on our dataset. However, our dataset is extremely small, therefore, it would most likely overfit. If it happened, then the models would be highly accurate on the data in the dataset, but they will be inaccurate or completely wrong for the data which are not in the dataset.

The second option is to use models based just on the physics laws (i.e., 'white box' approach), without any available data. Most constants and equations can be either found in the literature or calculated based on theoretical equations or correlations. However, deriving the model equation, finding all the constants and measuring all the dimensions would be challenging, extremely time consuming and likely not accurate enough in the end.

The third option is to use the 'grey box' approach. In this approach, we use the physics laws to describe major phenomena, but involved constants are found using numerical methods and measured data. We chose 'grey box' approach as it was best suited for our problem because this approach is general and the resulting models can be calibrated for various devices of the same nature.

In order to simulate the individual models as well as the whole device, we used NLCM (Non-Linear Continuous state space Models) toolbox [6]. This toolbox is mainly intended for simulation, calibration and control of non-linear continuous systems. However, it can be applied for finding the steady states of the system as well as for steady state optimization. In order to numerically find the steady states of the system, we inserted artificial dynamics into otherwise steady state models. True dynamics of the component are negligible compared to the rate of change of the outside air temperature and humidity. For modeling the heat pump, we utilized the VCC (Vapor Compression Cycle) toolbox [7]. This is a toolbox based on the NLCM toolbox, but it specializes in modeling vapor compression cycles. We took advantage mainly of the refrigerant properties wrapper of the REFPROP library [8] which is compatible with the NLCM toolbox.

For the description of individual models, we used notation which is common in control theory and in NLCM as well. This description uses internal states x, its derivative $f_c(x, u, \theta)$, parameters θ and the output function $y = g(x, u, \theta)$

$$\begin{aligned} \dot{x} &= f_c(x, u, \theta), \\ y &= g(x, u, \theta). \end{aligned} \tag{9}$$

Measured data (in Appendix A) will be used to find the parameters θ such that the sum of the square error of the steady state outputs of the individual systems is minimized.

$$\begin{aligned} \theta^* = \quad & \underset{x,\theta}{\arg\min} \quad \sum_{data} \left(g(x, u_{data}, \theta) - y_{data}\right)^2 \\ & s.t. \qquad f_c(x, u_{data}, \theta) = 0 \end{aligned} \tag{10}$$

2.1 Condenser

The condenser of the heat pump in AWG-DW is realized using a cross-counter flow fin-and-tube heat exchanger. In order to simplify the modeling of the heat exchanger, we assumed that the temperature gradient in the tube sections perpendicular to the airflow is negligible. Therefore, we modeled the heat exchanger as a counter-flow heat exchanger.

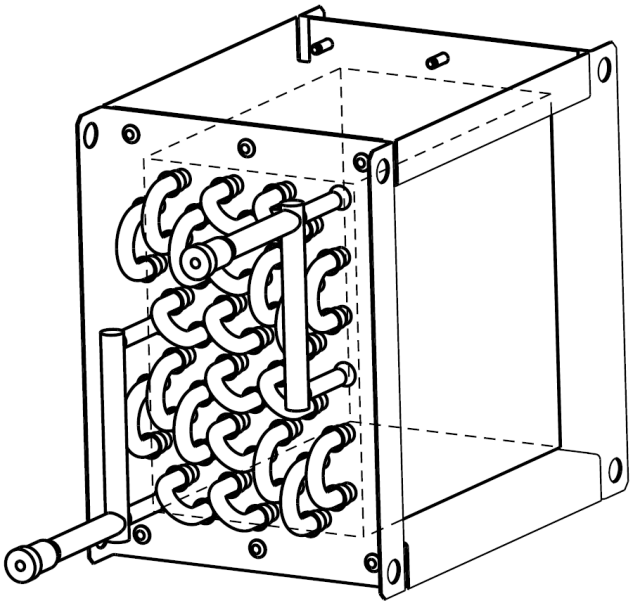

Figure 5: Drawing of the condenser used in AWG-DW

In the measured data (Appendix A), the output air temperature from the heat exchanger was higher than the saturation temperature of the refrigerant. Therefore a compartment model of the heat exchanger had to be used. In such a model, the condenser is split into three sections. In the first section, the refrigerant is a super-heated vapor. It transfers heat until it starts condensing. After that, in the condensing region, it condenses at a constant temperature until it is fully condensed. In the third section, the liquid refrigerant sub-cools.

The heat capacity of the refrigerant at constant pressure for the super-heated vapor as well as for the sub-cooled liquid changes with temperature as we can see in Fig. 6. In order to simplify the model, we considered the heat capacity to be the constant, equal to

$$c_{p,c} = \frac{H_i - H_o}{T_i - T_o} \tag{11}$$

in both the super-heat and sub-cool region of the heat exchanger. It is calculated as the enthalpy difference ($H_i - H_o$) in the participial region divided by the temperature difference ($T_i - T_o$). The disadvantage of this approach is that we need to know both the input and output enthalpy in the region before calculating the actual heat transfer.

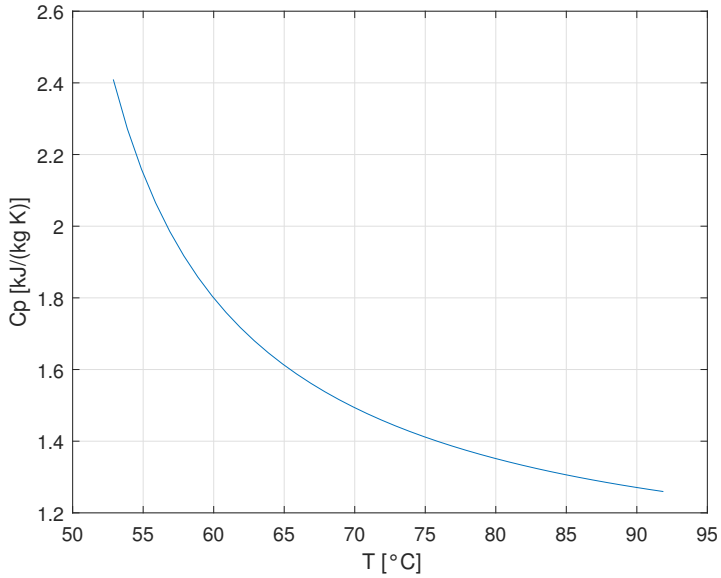

Figure 6: Heat capacity at constant pressure at 32 bar

2.1.1 Equation derivation

For the sub-cool and the super-heat region, we derive a model based on the differential equations for the counter-flowing fluids. The counter flow direction of the streams is already taken into account

$$\begin{aligned} \dot{V}_a \, c_a \, \rho_a \, \frac{\partial}{\partial x} T_a \left(x\right) &= -k \, \left(T_a \left(x\right) - T_r \left(x\right)\right), \\ c_r \, \dot{\mathrm{m}}_r \, \frac{\partial}{\partial x} T_r \left(x\right) &= -k \, \left(T_a \left(x\right) - T_r \left(x\right)\right). \end{aligned} \tag{12}$$

Therefore, both flow rates $\dot{m}_r$ as well as $\dot{V}_a$ are positive even though their directions are opposite. Heat transfer rate coefficient k is considered to be constant.

Solving Eq. (12) with size region d and boundary conditions: input refrigerant temperature $T_r(d) = T_{r,i}$ and the input air temperature $T_a(0) = T_{a,i}$ gives us the outlet temperatures of the air and the refrigerant in the region.

$$T_{a,o} = T_{\mathrm{r,i}} - \frac{\left(c_r \, \dot{\mathrm{m}}_r - \dot{V}_a \, c_a \, \rho_a\right) \left(T_{\mathrm{a,i}} - T_{\mathrm{r,i}}\right)}{\dot{V}_a \, c_a \, \rho_a - c_r \, \dot{\mathrm{m}}_r \, \mathrm{e}^{\frac{k \, d \left(c_r \, \dot{\mathrm{m}}_r - \dot{V}_a \, c_a \, \rho_a\right)}{\dot{V}_a \, c_a \, c_r \, \dot{\mathrm{m}}_r \, \rho_a}}} \tag{13}$$

$$T_{r,o} = T_{\mathrm{a,i}} - \frac{\left(c_r \, \dot{\mathrm{m}}_r - \dot{V}_a \, c_a \, \rho_a\right) \left(T_{\mathrm{a,i}} - T_{\mathrm{r,i}}\right)}{c_r \, \dot{\mathrm{m}}_r - \dot{V}_a \, c_a \, \rho_a \, \mathrm{e}^{-\frac{k \, d \left(c_r \, \dot{\mathrm{m}}_r - \dot{V}_a \, c_a \, \rho_a\right)}{\dot{V}_a \, c_a \, c_r \, \dot{\mathrm{m}}_r \, \rho_a}}} \tag{14}$$

Eq. (13) can be also modified to be used for the condensation region of the condenser. If the refrigerant is at its condensation temperature, then the temperature does not change, because the phase of the refrigerant changes. Those conditions can be modeled by assuming the heat capacity of the refrigerant is equal to infinity.

$$T_{a,o,c} = \lim_{c_r \to \infty} T_{a,o} = T_{\mathrm{r,i}} + \mathrm{e}^{-\frac{k \, x}{\dot{V}_a \, c_a \, \rho_a}} \left(T_{\mathrm{a,i}} - T_{\mathrm{r,i}}\right) \tag{15}$$

2.1.2 Model implementation

$c_{a,dry}$ specific heat capacity of dry air $\left[\mathrm{kJ\,K^{-1}\,kg^{-1}}\right]$
c_{wv} specific heat capacity of water vapor $\left[\mathrm{kJ\,K^{-1}\,kg^{-1}}\right]$
c_a specific heat capacity of moist air $\left[\mathrm{kJ\,K^{-1}\,kg^{-1}_{dry\ air}}\right]$
c_c mean specific heat capacity of refrigerant in sub-cool region $\left[\mathrm{kJ\,K^{-1}\,kg^{-1}}\right]$
c_h mean specific heat capacity of refrigerant in super-heat region $\left[\mathrm{kJ\,K^{-1}\,kg^{-1}}\right]$
X_a specific moisture of the air $\left[\mathrm{kg_{water\ vapor}/kg_{dry\ air}}\right]$
H_b bubbling point specific enthalpy of the refrigerant $\left[\mathrm{kJ\,kg^{-1}}\right]$
H_d dew point specific enthalpy of the refrigerant $\left[\mathrm{kJ\,kg^{-1}}\right]$
T_s refrigerant saturation temperature for given pressure $[^\circ\mathrm{C}]$
p_c refrigerant pressure $[\mathrm{bar}]$

The temperature of the refrigerant is determined by enthalpy and pressure. In AWG-DW, the liquid receiver is placed between the condenser region of the sub-cooler. This reservoir is considered to be big enough and to contain enough liquid refrigerant, so there is always a liquid as well as a gaseous refrigerant in this reservoir. This implies an important observation. In a steady state, the rate of condensation in the condenser region has to match the flow rate. The steady state boundary between the condensing region and the sub-cool region x_c is at a fixed position no matter the proprieties of input flows. The position of this boundary is defined by the position of the reservoir. The refrigerant can not be fully condensed before reaching the reservoir because there is not enough liquid refrigerant in the system to fill all that space. If the refrigerant was not fully condensed by the time it gets into the reservoir, it would mean either the reservoir does not contain liquid refrigerant anymore or a steady state is not achieved as the refrigerant level is still changing.

The refrigerant pressure is calculated numerically with a simple rule of thumb. If the refrigerant fully condenses before reaching the reservoir, the estimated pressure is too high. On the other hand, if the refrigerant does not fully condense when it reaches the reservoir, then the estimated pressure is too low.

A similar scheme can be used to find the steady state super-heat region size. If the refrigerant does not transfer enough energy in this region to start condensing, then the size of this region is too small. In the other case, if the refrigerant starts condensing while still in the super-heat region, this region is too big.

As already mentioned above, the compartment model of the condenser was implemented. The condenser with sub-cooler was divided into three sections. The position of the boundary between the super-heat region and the condensing region is called x_{sh} and the boundary between the condensing region and the sub-cooler is called x_c. The size of the condenser was normalized, so the total length of the condenser and the sub-cooler is equal to one.

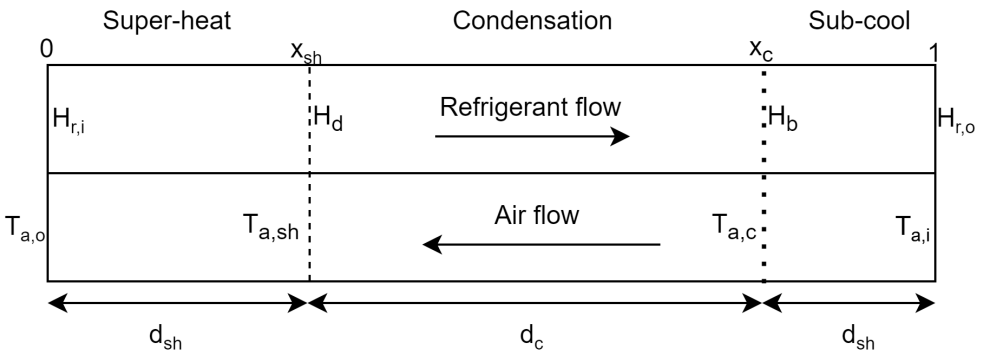

Figure 7: Diagram of three condenser regions

The model we developed for the condenser has five inputs: the enthalpy $H_{r,i}$ and mass flow rate $\dot{m}_r$ of the refrigerant, the temperature $T_{a,i}$, humidity $X_{a,i}$ and volumetric flow rate $\dot{V}_a$ of the air.

There are three internal variables: the super-heat region boundary position x_{sh}, the refrigerant pressure p_c and the output enthalpy H_o. There are two parameters: the position of the sub-cool x_c and the heat transfer coefficient k. The implemented model has six outputs: the enthalpy H_o, pressure p_c and mass flow $\dot{m}_r$ of the refrigerant and the temperature $T_{a,i}$, humidity X_a and volumetric flow rate $\dot{V}_a$ of the air. Some of the outputs ($\dot{m}_r$,X_a,$\dot{V}_a$) are unchanged inputs. This is done in case different modeling of this component will be implemented in the future.

NLCM toolbox [6] does not allow the limits on internal variables in the class template. Therefore, the limitations are done through their derivatives. This also means that we need to make sure all the variables are within their respective limits at the beginning of the calculation because the numerical algorithm can exceed those limits. We need to check that all the properties of the refrigerant are within limits specified by REFPROP [8] which is a tool for calculation of the refrigerant properties. We also needed to check the internal variables limits of the system to prevent errors. For example the positions of the boundary has to be within the limits and the output enthalpy has to be lower than the bubbling point enthalpy to prevent division by zero in Eq. (18).

$$H_{r,o} = min(H_{r,o}, H_b(p_c) - 1) \tag{16}$$

$$x_{sh} = min(0, max(x_{sh}, x_c)) \tag{17}$$

In the sub-cooler the capacities of the mediums (c_c, c_a) are calculated. Then we can get the air temperature $T_{a,sc}$ at the end of the sub-cooler from Eq. (13). The discrepancy $\Delta H_{r,o}$ between the estimated enthalpy difference $H_b(p_c) - H_{r,o}$ and the actual difference $\frac{Q_{sc}}{\dot{m}_r}$ is calculated to be later used as a derivative of the output enthalpy $H_{r,o}$

$$c_c = \frac{H_b(p_c) - H_{r,o}}{T_s(p_c) - T(H_{r,o}, p_c)} \tag{18}$$

$$c_a = c_{a,dry} + X_a c_{wv} \tag{19}$$

$$d_{sc} = 1 - x_c \tag{20}$$

$$T_{a,c} = T_s(p_c) - \frac{\left(c_c\,\dot{\mathrm{m}}_r - \dot{V}_a\,c_a\,\rho_a\right)\,(T_{\mathrm{a,i}} - T_s(p_c))}{\dot{V}_a\,c_a\,\rho_a - c_c\,\dot{\mathrm{m}}_r\,\mathrm{e}^{\frac{k\,d_{sc}\,(c_c\,\dot{\mathrm{m}}_r - \dot{V}_a\,c_a\,\rho_a)}{\dot{V}_a\,c_a\,c_c\,\dot{\mathrm{m}}_r\,\rho_a}}} \tag{21}$$

$$Q_{sc} = c_a\,(T_{a,sc} - T_{\mathrm{a,i}}) \tag{22}$$

$$\Delta H_{r,o} = H_b(p_c) - H_{r,o} - \frac{Q_{sc}}{\dot{m}_r} \tag{23}$$

We do the calculations in the condensing region as we did in the previous region. However, in this region, we used Eq. (15) to calculate the air temperature.

$$d_c = x_c - x_{sh} \tag{24}$$

$$T_{a,sh} = T_s(p_c) + \mathrm{e}^{-\frac{k\,d_c}{\dot{V}_a\,c_a\,\rho_a}}\,(T_{a,c} - T_c(p_c)) \tag{25}$$

$$Q_c = c_a\,(T_{a,sh} - T_{a,c}) \tag{26}$$

$$\Delta H_c = H_d(p_c) - H_b(p_c) - \frac{Q_c}{\dot{m}_r} \tag{27}$$

The super-heat region is almost the same as the sub-cooling region.

$$c_h = \frac{H_i - H_d(p_c)}{T(H_i, p_c) - T_s(p_c)} \tag{28}$$

$$d_{sh} = x_{sh} \tag{29}$$

$$T_{a,o} = T(H_i, p_c) - \frac{\left(c_h\,\dot{\mathrm{m}}_r - \dot{V}_a\,c_a\,\rho_a\right)\,(T_{a,c} - T(H_i, p_c))}{\dot{V}_a\,c_a\,\rho_a - c_h\,\dot{\mathrm{m}}_r\,\mathrm{e}^{\frac{k\,d_{sd}\,(c_h\,\dot{\mathrm{m}}_r - \dot{V}_a\,c_a\,\rho_a)}{\dot{V}_a\,c_a\,c_h\,\dot{\mathrm{m}}_r\,\rho_a}}} \tag{30}$$

$$Q_h = c_a\,(T_{a,o} - T_{a,c}) \tag{31}$$

$$\Delta H_{r,sh} = H_i(p_c) - H_d(p_c) - \frac{Q_h}{\dot{m}_r} \tag{32}$$

The artificial dynamic is created in such a way, that the steady state of this dynamic is the same as the steady state of the system. However, this dynamic does not describe the time dynamics of the real system. The artificial dynamics are based on logical principles. If the heat transfer in the super-heat region is too small, then the region is too small and vice versa. A similar logic was applied to the saturation pressure. If the heat transfer is too small, then the estimated saturation temperature (and therefore the saturation pressure) is too low and vice versa.

$$\dot{x}_{sh} = \Delta H_{r,sh} \tag{33}$$

$$\dot{p}_c = \Delta H_c \tag{34}$$

$$\dot{H}_{r,o} = \Delta H_{r,o} \tag{35}$$

We wanted to keep the internal variables within the limits, therefore we implemented few extra rules into the algorithm:

- $x_{sh} \leq 0 \Rightarrow \dot{x}_{sh} = max(-x_{sh}, \dot{x}_{sh})$
- $x_{sh} \geq x_c \Rightarrow \dot{x}_{sh} = min(x_c - x_{sh}, \dot{x}_{sh})$
- $p_c \leq p_{min} \Rightarrow \dot{p}_c = max(p_{min} - p_c, \dot{p}_c)$
- $p_c \geq p_{max} \Rightarrow \dot{p}_c = min(p_{max} - p_c, \dot{p}_c)$
- $H_{r,o} \leq H_b(p_c) \Rightarrow \dot{H}_{r,o} = max(H_b(p_c) - H_{r,o}, \dot{H}_{r,o})$
- $H_{r,o} \geq H_{max} \Rightarrow \dot{H}_{r,o} = min(H_{max} - H_{r,o}, \dot{H}_{r,o})$

2.1.3 Data analysis and model calibration

2.1.3.1 Air temperature at super-heat region boundary

In this subsection, we do a small thought experiment. We divide the condenser into two parts: the super-heat region and the rest. We denote the heat transfers in both parts as $\dot{Q}_1$ and $\dot{Q}_2$.

$$\dot{Q}_1 = c_a(T_{a,sh} - T_{a,i})\dot{m}_a = (H_d(p_c) - H_{r,o})\dot{m}_r \tag{36}$$

$$\dot{Q}_2 = c_a(T_{a,o} - T_{a,sh})\dot{m}_a = (H_{r,i} - H_d(p_c))\dot{m}_r \tag{37}$$

$$\dot{Q} = \dot{Q}_1 + \dot{Q}_2 = c_a(T_{a,o} - T_{a,i})\dot{m}_a = (H_{r,i} - H_{r,o})\dot{m}_r \tag{38}$$

We can express the air temperature at the boundary of the super-heat region and the condensing region by dividing Eq. (36) by Eq. (38). The advantage of this approach is that it allows us to analyze

the behavior of the heat exchanger without measuring the mass flow rate of neither the air nor the refrigerant.

The refrigerant flow rate was not directly measured. Still, it can be estimated either from the heat transfer in the evaporator or from compressor rotation speed and the pressure measurements. The condenser airflow was not directly measured either. It is estimated from the rotation speed of the ventilator. Therefore, this thought experiment experiments utilizes only the measurements that should have reasonable accuracy. The temperature

$$\frac{T_{a,sh} - T_{a,i}}{T_{a,o} - T_{a,i}} = \frac{H_d(p_c) - H_{r,o}}{H_{r,i} - H_{r,o}} \tag{39}$$

$$T_{a,sh} = T_{a,i} + (T_{a,o} - T_{a,i}) \frac{H_d(p_c) - H_{r,o}}{H_{r,i} - H_{r,o}} \tag{40}$$

The results of Eq. (40) can be seen in Table 1. Based on this calculation, the temperature at the boundary of the super-heat region should be almost equal to the condensation (saturation) temperature of the refrigerant. This in terms means that the condensing region behaves as a counter-flow heat exchanger with an efficiency of almost 100%. If the heat exchanger was reasonably sized, it should have never achieved such high efficiency. This suggests that there was an issue with the measured data. One possible way to explain this result is an incorrect measurement of the temperature $T(H_i, p_c)$ between the compressor outlet and the condenser inlet. The mounting of this sensor in in Fig. 8. Another possible explanation is that the calculated enthalpy $H_{r,o}$ at the condenser output is incorrect. If there was not enough refrigerant, the output refrigerant would not have to be fully condensed at the condenser output. The fact that the refrigerant temperature measured at the condenser output was lower than the saturation temperature could be explained by improper mounting of the sensor or by a shift of the saturation temperature due to the pressure drop in the condenser.

	$T_{a,i}$ [°C]	$T_{a,o}$ [°C]	$H_{a,i}$ [kJ/kg]	$H_{a,o}$ [kJ/kg]	$H_{r,o}$ [kJ/kg]	$H_{r,i}$ [kJ/kg]	H_d [kJ/kg]	$T_{a,c}$ [°C]	$T_s(p_c)$ [°C]
Exp 1	15.3	52	28	65.4	457	425	268	45.7	45.6
Exp 2	16.5	68.3	35.6	88.5	466	419	285	54.7	56
Exp 3	21.2	64.8	46.8	91.5	470	420	285	53.1	54.6
Exp 4	26.1	70.9	39	84.5	470	417	295	57.4	58
Exp 5	26.6	63.5	45.9	83.6	468	420	288	53.7	54.5
Exp 6	25.5	62.8	51.1	89.4	468	420	284	53	54.1
Exp 7	35.5	65.9	48.6	79.5	470	418	294	57	56.8
Exp 8	36.3	59.4	55.8	79.3	471	420	288	53	53.9
Exp 9	35.4	57.8	61.3	84.3	471	421	286	51.7	53
Exp 10	13.9	23.7	26.6	36.6	443	427	235	23	24
Exp 11	15.1	31.3	34.1	50.7	443	427	245	30.1	31.2
Exp 12	15.2	34.2	34.3	53.6	446	427	247	32.4	33.2
Exp 13	19.4	65.3	44.8	92	463	420	283	54.4	54.3
Exp 14	24.8	55.4	37.6	68.8	459	424	273	49.6	48.3
Exp 15	24.9	71.7	44.1	91.9	466	417	292	58.3	58.3
Exp 16	25.5	65.3	51.1	92	465	419	287	55.1	55.5
Exp 17	35.7	64.2	48.8	77.7	466	419	291	56.5	56
Exp 18	35.4	58	54.9	78	463	421	286	52.7	52.8
Exp 19	35.2	57.8	61.1	84.2	464	421	286	52.3	53.1
Exp 20	25.4	62.3	51	88.8	463	420	284	53.5	53.9
Exp 21	34	60.7	53.4	80.7	464	421	286	54.2	53.7
Exp 22	35.7	60.3	61.6	86.8	467	420	288	53.9	54.3

Table 1: Air temperature in condenser at super-heat region boundary (selected data from Appendix A)

2.1.3.2 Air flow rate

We also investigated the energy balance of the condenser in the heat pump. The refrigerant flow rate in the heat pump was not measured directly. Therefore, we used the theoretical flow rate calculated from the heat transfer rate in the evaporator $\dot{m}_{r,e}$. Using the conservation of energy

$$(H_{a,o} - H_{a,i})\,\dot{m}_a = (H_{r,i} - H_{r,o})\,\dot{m}_r, \tag{41}$$

we can calculate the theoretical air flow rate. Enthalpies of the air we acquired from the COOLPROP [9] library, to reduce the possibility of an error and to increase the accuracy. Enthalpy of the refrigerant R410a was acquired with REFPROP program [8].

In Table 2, we can see that the theoretical flow rates in the refrigerant are lower than those in the evaporator. This is clearly some sort of measurement problem as the air flows through the condenser, some of it is then let out through the control air valve and the rest passes through the evaporator. One way to explain these results is the refrigerant mass flow rate in the evaporator (see explanation in Section 2.2.4) is incorrectly estimated. The other explanation is that the inlet refrigerant temperature and, therefore, the enthalpy is incorrect due to incorrect sensor mounting.

	$T_{r,i}$ [°C]	$T_{r,o}$ [°C]	$\dot{V}_{a,c,t}$ [m^3/h]	$\dot{V}_{a,e,m}$ [m^3/h]	$H_{a,i}$ [kJ/kg]	$H_{a,o}$ [kJ/kg]	$H_{r,i}$ [kJ/kg]	$H_{r,o}$ [kJ/kg]	$\dot{m}_{r,e}$ [kg/h]
Exp 1	65.7	40.3	119	120	28	65.4	457	268	28.2
Exp 2	81.5	49.7	113	120	35.6	88.5	466	285	39.7
Exp 3	82.8	49.4	152	120	46.8	91.5	470	285	44.1
Exp 4	85.7	54.1	90.7	120	39	84.5	470	295	28.4
Exp 5	81.7	50.7	133	120	45.9	83.6	468	288	33.4
Exp 6	81.3	49.1	153	120	51.1	89.4	468	284	38.2
Exp 7	84.7	53.7	109	119	48.6	79.5	470	294	23.1
Exp 8	83	50.9	189	115	55.8	79.3	471	288	29.3
Exp 9	82.6	49.9	190	97.3	61.3	84.3	471	286	28.3
Exp 10	35.7	21.3	91	113	26.6	36.6	443	235	5.27
Exp 11	42.1	27.5	107	120	34.1	50.7	443	245	10.8
Exp 12	46.5	28.8	117	120	34.3	53.6	446	247	13.6
Exp 13	77.7	48.2	100	120	44.8	92	463	283	31.5
Exp 14	69.2	43.3	81.8	120	37.6	68.8	459	273	16.5
Exp 15	83.7	53.1	81.5	120	44.1	91.9	466	292	27
Exp 16	79.9	50.5	106	120	51.1	92	465	287	29.4
Exp 17	81.1	52.5	96.2	120	48.8	77.7	466	291	19.2
Exp 18	76.6	49.6	128	120	54.9	78	463	286	19.9
Exp 19	77.6	49.7	150	115	61.1	84.2	464	286	23.4
Exp 20	77.4	49	127	120	51	88.8	463	284	32.2
Exp 21	77.8	49.8	122	120	53.4	80.7	464	286	22.5
Exp 22	80.4	50.9	164	120	61.6	86.8	467	288	27.8

Table 2: Theoretical air flow rate in the condenser (selected data from Appendix A)

Figure 8: Improper installation of the temperature sensor at the refrigerant line

2.1.3.3 Calibration

In Section 2.3.2 we investigated the temperature measured at the output of the compressor and we also compared the theoretical refrigerant flow rates. We found evidence that the measurement of the temperature and the enthalpy of the refrigerant at the input and output might not be correct. Due to the high uncertainty concerning the accuracy of the measured and calculated data, we could not calibrate the system and expect the calibration to be accurate. However, we did the calibration anyways to be able to progress in the project. The theoretical mass flow rate in the evaporator was used and the airflow rate was calculated to keep the heat transfer in both mediums the same. We took the theoretical refrigerant enthalpy and temperatures which we calculated as the compressor output in Section 2.3.2 as the input to the condenser. This way, we get a model which is not just a 100 % efficient heat exchanger. The measured values are denoted with '*m*' subscription and the theoretical ones based on the model have subscription '*t*'. The calibration achieved reasonable accuracy. The root mean square error of the temperature is $0.7\,^{\circ}\mathrm{C}$ and of the pressure $1.1\,\mathrm{bar}$.

	$\dot{m}_{r,e}$ [kg/h]	X_A [g/kg]	$\dot{V}_a$ [m^3/h]	$H_{r,o}$ [kJ/kg]	$H_{r,o,t}$ [kJ/kg]	$p_{r,m}$ [bar]	$p_{r,t}$ [bar]	$T_{a,o,m}$ [°C]	$T_{a,o,t}$ [°C]
Exp 1	28.2	5	0.0361	268	262	27.7	26.8	52	53.1
Exp 2	39.7	7.5	0.0341	285	281	35.1	33.1	68.3	69
Exp 3	44.1	10	0.0443	285	282	34.1	32.4	64.8	65.5
Exp 4	28.4	5	0.0274	295	287	36.7	35.9	70.9	71.6
Exp 5	33.4	7.5	0.0393	288	283	34	33	63.5	64.5
Exp 6	38.2	10	0.0451	284	282	33.7	32.3	62.8	63.3
Exp 7	23.1	5	0.0326	294	289	35.8	35.4	65.9	66.3
Exp 8	29.3	7.5	0.0549	288	285	33.5	32.7	59.4	59.8
Exp 9	28.3	10	0.055	286	282	32.8	31.8	57.8	58.3
Exp 10	5.27	5	0.0274	235	225	16.1	15.6	23.7	24.1
Exp 11	10.8	7.5	0.0333	245	235	19.5	18.5	31.3	32.1
Exp 12	13.6	7.5	0.036	247	239	20.5	19.6	34.2	34.9
Exp 13	31.5	10	0.0306	283	278	33.8	32.5	65.3	66.1
Exp 14	16.5	5	0.0253	273	266	29.5	29.4	55.4	56.5
Exp 15	27	7.5	0.0252	292	286	37	35.8	71.7	71.8
Exp 16	29.4	10	0.0324	287	282	34.7	33.4	65.3	66
Exp 17	19.2	5	0.0296	291	285	35.1	34.7	64.2	64.4
Exp 18	19.9	7.5	0.0387	286	280	32.7	32	58	58.7
Exp 19	23.4	10	0.0454	286	281	32.9	31.8	57.8	58.3
Exp 20	32.2	10	0.0384	284	280	33.5	32.2	62.3	63
Exp 21	22.5	7.5	0.0369	286	282	33.4	32.9	60.7	61.2
Exp 22	27.8	10	0.0487	288	285	33.8	33	60.3	60.7

Table 3: Results of the condenser calibration

2.2 Evaporator

The evaporator is the second heat exchanger in the heat pump system. The refrigerant comes into the evaporator from the expansion valve in a mixed state. The refrigerant gains heat, evaporates and then turns into a super-heated vapor. The air flowing through the evaporator gives heat to the refrigerant and its temperature decreases. In AWG-DW, we want the temperature of the evaporator below the dew point temperature of the air to produce water. The liquid water is then collected into a storage tank.

Many researchers (e.g. [10–13]) focused on modeling the fin-and-tube heat exchanger under dehumidifying conditions of the moist air. When the temperature on the surface of the heat exchanger is lower than the dew point of the air, the water vapor in the air condensates. The water condensation adds one more variable to the equations and thus makes the resulting model more complicated compared with the condenser model. Many models of the evaporator use some sort of discretization along the airflow direction.

One of the challenges in modeling such systems is that the surface temperature can be below the dew temperature only at certain parts of the heat exchangers fins. This can happen when the temperature at the root of the fin is below the dew temperature of the air while the temperature at the tip of the fin is still above the dew temperature.

Many of these models [10,11] are based on the principles presented by Threlkeld [12]. He assumes that the heat transferred into the heat exchanger is proportional to the enthalpy difference between the flowing air and the saturated moist air at a temperature equal to heat exchanger's surface.

2.2.1 Equivalent dry bulb temperature method

Wang and Hihara developed a method called 'equivalent dry bulb temperature' (EDT) [13]. The basic principles are similar to those proposed by Threlkeld [12]. The difference between them is that they convert the dehumidification process (1-2-3 line in Fig. 9) into one without mass transfer but with a different temperature (1^e-2^e-3 line in Fig. 9). Those new points on the psychometric chart have the same enthalpy as the original ones but they have the same specific humidity as saturated moist air at the temperature of the heat exchangers surface. The resulting temperature of this point is called equivalent dry bulb temperature (EDT), hence the name of this method. Heat exchanges are then calculated with no mass transfer. The NTU theory can be therefore utilized. The output air (2) has the same enthalpy as its EDT equivalent (2^e). The output air point in the psychometric chart (2) is on a straight line between points 1 and 3 on the psychometric chart.

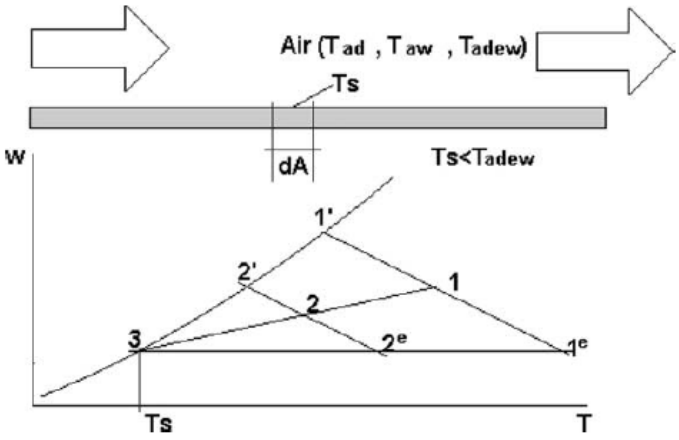

Figure 9: Cooling and dehumidifying of moist air over a flat plate with constant surface temperature [13]

However, we encountered a problem when modeling the evaporator with the EDT method. In some cases, when the input humidity was already quite high, the line between points 1 and 3 would cross the line 2^e $2'$ above the saturation line. The resulting point 2 should then theoretically have relative humidity over 100 %. We made an exception for this situation. If this happens, the resulting output air has the same enthalpy and 100 % relative humidity.

Even with this modification, the resulting model did not accurately describe the measured data. The output relative humidity was always higher than the measured data. The issue here is that the ratio of the latent heat and the total heat transferred is determined by the line connecting the point on the saturation line 3 and the original point 1. Even though many researchers made similar assumptions, it does not result in a good description of the measured data in our case.

2.2.2 Model based on actual dry bulb temperature method

c_a	specific heat capacity of air $\left[\mathrm{kJ\,K^{-1}\,kg^{-1}}\right]$
$k_{T,t}$	heat transfer coefficient of the tube $\left[\mathrm{kJ\,K^{-1}\,m^{-2}\,s^{-1}}\right]$
$k_{T,f}$	heat transfer coefficient of the fin $\left[\mathrm{kJ\,K^{-1}\,m^{-2}\,s^{-1}}\right]$
$k_{T,a}$	heat transfer coefficient of the air $\left[\mathrm{kJ\,K^{-1}\,m^{-2}\,s^{-1}}\right]$
k_T	total heat transfer coefficient $\left[\mathrm{kJ\,K^{-1}\,m^{-2}\,s^{-1}}\right]$
k_X	mass transfer coefficient $\left[\mathrm{kg\,m^{-2}\,s^{-1}}\right]$
$H_{s,w}$	enthalpy of saturated moist air at the temperature of the water film $\left[\mathrm{kJ\,kg^{-1}}\right]$
H_a	enthalpy of the air $\left[\mathrm{kJ\,kg^{-1}}\right]$
$H_{g,w}$	enthalpy of the water vapor in the air temperature $\left[\mathrm{kJ\,kg^{-1}}\right]$
$H_{l,w}$	enthalpy of liquid water at the temperature of the water film $\left[\mathrm{kJ\,kg^{-1}}\right]$
H^0_{wv}	enthalpy of the water vapor at 0 °C $\left[\mathrm{kJ\,kg^{-1}}\right]$
$T_{s,w}$	temperature of the water film [°C]
T_a	temperature of the air [°C]
p_e	refrigerant pressure [bar]

The basic principles for the actual dry bulb temperature method were laid down by Threlkeld [12]. According to Threlkeld, the heat transferred into the water film at the surface of the heat exchanger is

$$d\dot{Q} = \left(k_{T,a}(T_a - T_{s,w}) + k_X(X_a - X_{s,w})(H_{g,w} - H_{l,w})\right) dA. \tag{42}$$

Neglecting the change in heat capacity due to the water content change, the enthalpy of the moist air is then approximated by

$$H = c_a t + H^0_{wv}. \tag{43}$$

The specific heat capacity of the water vapor in the moist air is neglected and the enthalpy of the water vapor is considered independent on the air temperature.

Eq. (42) can be rearranged with Eq. (43) into

$$d\dot{Q} = \left(\frac{k_{T,a}}{c_a}(H_a - H_{s,w}) + \frac{k_{T,a}}{\mathrm{Le}}(X_a - X_{s,w})(H_{g,w} - H_{l,w} - LeH^0_{wv}\right) dA, \tag{44}$$

$$\mathrm{Le} = \frac{k_{T,a}}{k_X c_a}. \tag{45}$$

Threlkeld then argued that the second component on the right-hand side of Eq. (44) is relatively small compared to the first one. This is a logical solution because the Lewis number Le is approximately equal to 1 for moist air [14]. $H_{g,w} - H_{l,w}$ as well as H^0_{wv} is basically the latent heat of vaporization. The main reason for this simplification is the possibility of expressing the heat transfer as the function

of just the enthalpy difference $(H_a - H_{s,w})$. However, we decided not to use this simplification as we were more focused on the dehumidification rather than the heat transfer.

Many models of the dehumidification processes neglect the influence of condensing water on the temperature of the surface of the heat exchanger (to be exact the temperature of the water film). We took this assumption as well. We can separate the heat transfer $(k_{T,a}(T_a - T_{s,w}))$ from the mass transfer because the surface temperature is considered independent of the latent heat of water condensation. We can express the on the surface

$$\left(\frac{1}{k_{T,t}} + \frac{1}{k_{T,f}}\right)(T_{surf} - T_r) = \frac{1}{k_{T,a}}(T_a - T_{sufr}). \tag{46}$$

However, the mass transfer is still dependent on the surface temperature and, therefore, the temperature of the air and refrigerant.The heat transfer due to the temperature difference can be then expressed as

$$\begin{aligned} \dot{Q}_t &= k_T\left(T_a - T_r\right), \\ \frac{1}{k_T} &= \frac{1}{k_{T,t}} + \frac{1}{k_{T,f}} + \frac{1}{k_{T,a}}. \end{aligned} \tag{47}$$

The mass transfer in the direction of air flow x is derived from the difference absolute humanities based on the Fick's law

$$d\dot{m}_w = \dot{V}_a \rho_a dX_a = Ak_X \max(0, X_s(T_{surf}) - X_a)dx, \tag{48}$$

$$\frac{dX_a}{dx} = \frac{Ak_X}{\dot{V}_a \rho_a} \max(0, X_s(T_{surf}) - X_a). \tag{49}$$

The maximum in Eq. (49) describes the mass transfer rate when the surface temperature is lower than the dew temperature. We neglected the temperature difference on the fins. Therefore, the situation when the temperature of only a part of the fins is below the dew point temperature was not considered.

The resulting model still follows the basic principles of enthalpy difference. However, the ratio of latent heat and total heat transferred is different compared with EDT and this ratio is also adjustable with the system parameters.

2.2.3 Model implementation

While developing the evaporator model, we decided to split the evaporator into two compartments similarly as we did in the condenser model. The first region is the evaporation region, where the refrigerant evaporates until it is entirely gaseous. In the second region, the refrigerant super-heats. The evaporator is a counter-flow heat exchanger, therefore, the air flows first into the super-heat region and then into the evaporating region.

The evaporator is divided into those two regions by evaporation region boundary position x_e. The total size of the evaporator along the flow axis is normalized so that it is equal to one.

The refrigerant temperature in the evaporation region is equal to the saturated temperature. In the super-heat region, we assume the temperature to be constant, equal to its mean temperature. This is the average between the saturated temperature and the output temperature of the refrigerant.

The evaporator model that we created has six inputs, two internal variables and seven outputs. Inputs consists of the properties of the refrigerant and air streams: the input enthalpy $H_{r,i}$, pressure P_r and mass flow $\dot{m}_r$ of the refrigerant and the temperature $T_{a,i}$, specific humidity $X_{a,i}$ and volumetric flow rate $\dot{V}_a$ of the air.

Two internal variables are the evaporation region boundary position x_e and the output enthalpy $H_{r,o}$.

At the output, we implemented the produced liquid water mass flow rate $\dot{m}_w$ and the properties of the refrigerant $H_{r,o}$, p_r, $\dot{m}_r$ and air outlet properties $T_{a,o}$, $X_{a,o}$, $\dot{V}_a$. The flow rates and the refrigerant pressure are outputted unchanged, in case different model of this component will be implemented in the future.

As we already mentioned, the internal states can not be directly limited, therefore it is kept within the bounds using its derivatives. However, numerical algorithms can exceed the specified limitations, therefore internal variables as well as inputs has to be checked at the beginning of the calculation.

$$H_{r,o} = max(H_{min}, min(H_{max}, H_{r,o})) \tag{50}$$
$$x_e = max(0, min(1, x_e)) \tag{51}$$

In both regions, the temperature of the air can be calculated using Eq. (15) which we derived earlier. For the super-heater section, the temperature is calculated

$$\begin{aligned} T_{a,sh}(x) &= T_{r,sh} + \mathrm{e}^{-\frac{k_T x}{\dot{V}_a c_a \rho_a}} (T_{\mathrm{a,i}} - T_{r,sh}) \qquad 0 \le x \le d_{sh}, \\ T_{r,sh} &= \frac{T_s(p_e) + T_r(H_{r,o}, p_e)}{2}, \\ d_{sh} &= 1 - x_e. \end{aligned} \tag{52}$$

The output air specific humidity is acquired by solving Eq. (49) using the forward Euler method. The calculation is then done identically in the evaporation region. This way we get the output air temperature $T_{a,o}$ and specific humidity $X_{a,o}$

The heat transferred in both regions is derived

$$\dot{Q}_{sh} = c_a(T_{a,i} - T_{a,sh}) + H^0_{wv}(X_{a,i} - X_{a,sh}) \tag{53}$$
$$\dot{Q}_e = c_a(T_{a,sh} - T_{a,o}) + H^0_{wv}(X_{a,sh} - X_{a,o}) \tag{54}$$

The discrepancy between the estimated enthalpy difference and the actual one is calculated

$$\Delta H_{r,o} = H_d - H_{r,o} - \frac{\dot{Q}_{sh}}{\dot{m}_r}, \tag{55}$$
$$\Delta H_{r,e} = H_{r,i}d - H_d - \frac{\dot{Q}_e}{\dot{m}_r}. \tag{56}$$

The mass flow rate of liquid water is

$$\dot{m}_w = (X_{a,i} - X_{a,o})\ \dot{V}_a\, \rho_a. \tag{57}$$

The artificial dynamics are created in such a way, that the steady state of this dynamics is the same as the steady state of the system. However, this dynamics do not describe the time dynamic of the real system. The artificial dynamics is based on logical principles. If the heat transfer in the evaporation region is too small, then the region is too small and vice versa.

$$\dot{x}_e = \Delta H_{r,e} \tag{58}$$
$$\dot{H}_{r,o} = \Delta H_{r,o} \tag{59}$$

2.2.4 Data analysis and model calibration

The water generation in AWG-DW was measured manually in each experiment. To check the consistency of the data, we decided to compare the theoretical water generation based on Eq. (57) with the amount of water that was found in the reservoir at the end of each experiment. The results are shown in Table 4. The calculated data roughly corresponds to the measured data.

	$X_{a,c,i}$ [g/kg]	$X_{a,c,o}$ [g/kg]	$\dot{V}_{a,e}$ [m^3/h]	$\dot{m}_{w,t}$ [kg/h]	$\dot{m}_{w,m}$ [kg/h]	$\dot{m}_{w,t}/\dot{m}_{w,m}$ [−]
Exp 1	13.3	5.88	120	1.07	0.91	1.18
Exp 2	16.4	6.41	120	1.44	1.23	1.17
Exp 3	19.1	7.38	120	1.69	1.45	1.17
Exp 4	13.2	7.23	120	0.853	0.75	1.14
Exp 5	15.8	7.68	120	1.17	1	1.17
Exp 6	17.1	7.26	120	1.42	1.25	1.14
Exp 7	12	7.83	119	0.604	0.55	1.1
Exp 8	15.2	8.29	115	0.953	0.807	1.18
Exp 9	16.8	7.95	97.3	1.03	0.953	1.08
Exp 10	5.76	4.62	113	0.156	0.229	0.679
Exp 11	7.9	5.12	120	0.4	0.483	0.829
Exp 12	8.33	4.77	120	0.512	0.577	0.887
Exp 13	14.4	6.45	120	1.15	1.18	0.975
Exp 14	9.06	5.77	120	0.475	0.383	1.24
Exp 15	12.2	6.38	120	0.837	0.9	0.93
Exp 16	13.6	6.65	120	0.999	0.99	1.01
Exp 17	9.23	6.51	120	0.392	0.333	1.18
Exp 18	10.9	7.2	120	0.536	0.513	1.04
Exp 19	12.8	7.25	115	0.765	0.821	0.932
Exp 20	15.1	7.08	120	1.16	1.33	0.873
Exp 21	12.1	7.3	120	0.692	0.78	0.887
Exp 22	14.5	8.05	120	0.923	0.922	1

Table 4: Water generation comparison

For the comparison in Section 2.3.2, we calculated the theoretical flow rate of the refrigerant in the evaporator. To reduce the error, we utilized the COOLPROP library to calculate the enthalpy of the air $H_a\left(T, X\right)$ and the condensed water $H_w\left(T\right)$. The total heat transfer based on the measured data is defined

$$\dot{Q}_e = \left(H_a\left(T_{a,i}, X_{a,i}\right) - H_a\left(T_{a,o}, X_{a,o}\right)\right)\dot{V}_a\,\rho_a - H_w\left(T_{surf}\right)\dot{m}_w \tag{60}$$

The theoretical mass flow rate of the refrigerant is

$$\dot{m}_r = \frac{\dot{Q}_e}{H_{r,o} - H_{r,i}}. \tag{61}$$

The resulting mass flow rate is shown in Table 5. The measured values are denoted with 'm' subscription and the theoretically calculated ones have subscription 't'. Calculations in Sections 2.1.3.2 and 2.3.2 suggest that the mass flow rate in the evaporator might be incorrect. The input enthalpy of the evaporator is taken from the measurement at the output of the condenser. We suspect that this enthalpy is not right due to a lack of refrigerant in the heat pump. The explanation for this is in Section 2.1.3.2

2.2.4.1 Calibration

Optimal parameters were found in order to minimize the model error. The calibration results are shown in Table 5. The calibration achieved reasonable accuracy. The root means square error of the temperature is $1.1\,°\mathrm{C}$ and of the absolute humidity $0.7\,\mathrm{g\,kg^{-1}}$.

	$H_{r,i}$ [kJ/kg]	p_r [bar]	$\dot{m}_r$ [kg/h]	$T_{a,i}$ [°C]	$X_{a,i}$ [g/kg]	$\dot{V}_a$ [m^3/h]	$T_{a,o,m}$ [°C]	$T_{a,o,t}$ [°C]	$X_{a,o,m}$ [g/kg]	$X_{a,o,t}$ [g/kg]
Exp 1	268	8.52	28.2	20	13.3	120	6.72	8.92	5.88	6.29
Exp 2	285	8.46	39.7	23	16.4	120	8.09	9.92	6.41	6.91
Exp 3	285	8.76	44.1	25.4	19.1	120	10.2	11.5	7.38	7.76
Exp 4	295	8.45	28.4	22.3	13.2	120	10.4	9.87	7.23	6.53
Exp 5	288	8.67	33.4	24.1	15.8	120	11.2	10.9	7.68	7.16
Exp 6	284	8.6	38.2	24.2	17.1	120	10.1	10.7	7.26	7.19
Exp 7	294	8.42	23.1	23	12	119	11.6	11	7.83	6.75
Exp 8	288	8.54	29.3	25.3	15.2	115	12.5	11.3	8.29	7.26
Exp 9	286	8.28	28.3	24.9	16.8	97.3	12.2	9.34	7.95	6.92
Exp 10	235	8.1	5.27	8.66	5.76	113	3.96	3.95	4.62	4.42
Exp 11	245	8.28	10.8	11.8	7.9	120	4.85	5.2	5.12	4.91
Exp 12	247	8.11	13.6	12.6	8.33	120	4.2	5.1	4.77	4.85
Exp 13	283	8.41	31.5	20.5	14.4	120	8.16	8.86	6.45	6.43
Exp 14	273	8.08	16.5	16.5	9.06	120	6.84	6.83	5.77	5.2
Exp 15	292	8.22	27	19.5	12.2	120	8.27	8.1	6.38	5.94
Exp 16	287	8.23	29.4	20.7	13.6	120	8.86	8.55	6.65	6.24
Exp 17	291	7.84	19.2	20.7	9.23	120	9.12	8.89	6.51	5.48
Exp 18	286	8.18	19.9	20.9	10.9	120	10.3	9.67	7.2	6.24
Exp 19	286	8.22	23.4	21.1	12.8	115	10.5	9.14	7.25	6.48
Exp 20	284	8.52	32.2	22.3	15.1	120	9.78	9.82	7.08	6.75
Exp 21	286	8.3	22.5	20.9	12.1	120	10.4	9.52	7.3	6.48
Exp 22	288	8.65	27.8	23.4	14.5	120	11.8	10.9	8.05	7.2

Table 5: Evaporator calibration results

2.3 Compressor

η_{ie}	isentropic efficiency without motor $[-]$
η_{cie}	isentropic efficiency including motor $[-]$
η_V	volumetric efficiency including motor $[-]$
n_{RPM}	shaft speed $[RPM]$
ϕ_{MVR}	volume ratio of the main suction port $[-]$
ϕ_{AVRD}	volume ratio difference of the auxiliary port $[-]$
p_s	suction pressure $[\text{MPa}]$
p_d	discharge pressure $[\text{MPa}]$
p_a	auxiliary pressure $[\text{MPa}]$
v_s	specific volume at the suct. port $\left[\text{m}^3\,\text{kg}^{-1}\right]$
v_{die}	specific volume after the isentropic compression $\left[\text{m}^3\,\text{kg}^{-1}\right]$
V_s	main suction port displacement $\left[\text{m}^3/\text{rev}\right]$
V_a	auxiliary suction port displacement $\left[\text{m}^3/\text{rev}\right]$
γ	isentropic compression exponent $[-]$

The compressor is a part of the heat pump where the pressure of the refrigerant is increased.

Even though there are many types of compressors, most models use analogies with the piston compressor. The mass transfer of refrigerant in the compressor is determined by Eq. (62). In real compressors, there are leaks and output clearances which reduce the refrigerant flow rate. The volumetric efficiency η_V of the compressor includes all those inefficiencies.

$$\dot{m}_r = \frac{1}{v_s}\frac{n_{\text{RPM}}}{60}V_s\eta_V \tag{62}$$

The ideal (isentropic) compression process is reversible, so the entropy is constant. In this process, the pressure, temperature and enthalpy of the refrigerant are increased. The isentropic efficiency of the compressor is then calculated by comparing the enthalpy increase of the isentropic compressor with the real one

$$\eta_{ie} = \frac{H_{die} - H_s}{H_d - H_s}. \tag{63}$$

This equation does not account for any heat transfer, so in case the refrigerant is cooled during the compression the theoretical resulting isentropic efficiency can be over 100%. If we consider the efficiency of the electric motor, we can define the isentropic efficiency η_{cie} of the whole machine

$$\eta_{cie} = \frac{\dot{m}_r\left(H_{die} - H_s\right)}{P_{\text{comp}}}. \tag{64}$$

Neglecting the heat transfer between the housing of the compressor and the surrounding air then all the energy, which goes into the compressor has to be transferred into the refrigerant. Taking this assumption, the output enthalpy of the refrigerant is determined by

$$P_{\text{comp}} = \frac{\left(H_d - H_s\right)}{\dot{m}_r}. \tag{65}$$

Many compressor models are based on polynomial fits of measured data for the particular compressor. One of such polynomials was created by Erickson [15]. The volumetric efficiency polynomial is

$$\begin{aligned}\eta_V = {} & A_0 + A_1 n_{\mathrm{RPM}} + A_2 n_{\mathrm{RPM}}^2 + A_3 \phi_{\mathrm{MVR}} + A_4 \phi_{\mathrm{MVR}}^2 + A_5 \phi_{\mathrm{MVR}} n_{\mathrm{RPM}} \\ & + A_6 \phi_{\mathrm{AVRD}} + A_7 \phi_{\mathrm{AVRD}} \phi_{\mathrm{MVR}} + A_8 \phi_{\mathrm{AVRD}} n_{\mathrm{RPM}} + A_9 \phi_{\mathrm{AVRD}}^2 n_{\mathrm{RPM}} \\ & + A_{10} \phi_{\mathrm{AVRD}} n_{\mathrm{RPM}}^2 + A_{11} p_d\end{aligned} \tag{66}$$

The

$$\begin{aligned}\eta_{cie} = {} & C_0 + C_1 n_{\mathrm{RPM}} + C_2 n_{\mathrm{RPM}}^2 + C_3 \phi_{\mathrm{MVR}} + C_4 \phi_{\mathrm{MVR}}^2 + C_5 \phi_{\mathrm{MVR}} n_{\mathrm{RPM}} \\ & + C_6 \phi_{\mathrm{AVRD}} + C_7 \phi_{\mathrm{AVRD}} \phi_{\mathrm{MVR}} + C_8 \phi_{\mathrm{AVRD}} n_{\mathrm{RPM}} + C_9 \phi_{\mathrm{AVRD}}^2 n_{\mathrm{RPM}} \\ & + C_{10} \phi_{\mathrm{AVRD}} n_{\mathrm{RPM}}^2 + C_{11} p_d,\end{aligned} \tag{67}$$

where

$$\phi_{\mathrm{MVR}} = \left(\frac{p_d}{p_s}\right)^{\frac{1}{\gamma}} \tag{68}$$

$$\phi_{\mathrm{AVRD}} = \frac{V_a}{V_s} - \left(\frac{p_s}{p_a}\right)^{\frac{1}{\gamma}} \tag{69}$$

$$\gamma = \frac{ln(p_d) - ln(p_s)}{ln(v_s) - ln(v_{die})} \tag{70}$$

This model describes compressors with an economizer, however, it can be used for compressors without it as well. The coefficients associated with the auxiliary port and the economizer are removed

$$\eta_V = A_0 + A_1 n_{\mathrm{RPM}} + A_2 n_{\mathrm{RPM}}^2 + A_3 \phi_{\mathrm{MVR}} + A_4 \phi_{\mathrm{MVR}}^2 + A_5 \phi_{\mathrm{MVR}} n_{\mathrm{RPM}}, \tag{71}$$

$$\eta_{cie} = C_0 + C_1 n_{\mathrm{RPM}} + C_2 n_{\mathrm{RPM}}^2 + C_3 \phi_{\mathrm{MVR}} + C_4 \phi_{\mathrm{MVR}}^2 + C_5 \phi_{\mathrm{MVR}} n_{\mathrm{RPM}}. \tag{72}$$

2.3.1 Model implementation

The compressor in AWG-DW is controlled by a variable speed driver with an IGBT inverter. The energy losses in the inverter are transferred to the surrounding air rather than to refrigerant, therefore we had to take this into the account while modeling the compressor. We assumed the efficiency of the compressor inverter η_{inv} to be constant

$$\eta_{inv} = \frac{P_{comp}}{P_{in}}. \tag{73}$$

Our implemented model of the compressor has no internal variables, four inputs and five outputs. The model inputs are the suction (input) enthalpy H_s, pressure p_s, mas flow rate $\dot{m}_r$ and the discharge (output) pressure p_d. The output are discharge (input) enthalpy H_d, pressure p_d, mas flow rate $\dot{m}_r$, the rotation speed of the compressor n_{RPM} and the input electric power to compressor inverter P_{in}. The parameters are the polynomial coefficients $A_0...A_5$, $C_0...C_5$ and the efficiency of the inverter η_{inv}.

We were able to acquire the polynomial coefficients $A_0...A_5$, $C_0...C_5$ for the compressor which is used in AWG-DW, but for the R32 refrigerant. However, since both the R32 and R410A are high pressure refrigerants, we decided to use those coefficients in our model. The compressor discharge pressures and rotation speed are limited by its operation envelope, which can be seen in Fig. 10.

Due to our choice of input parameters for the heat pump system, we had to solve a cubic equation, which resulted from the combination of Eqs. (62) and (71). In order to solve this problem, we implemented the Cardano formula [16].

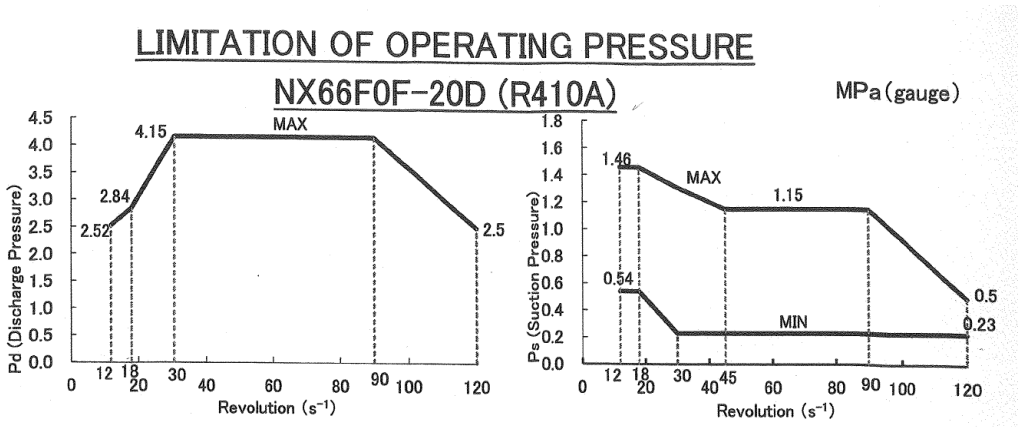

Figure 10: Operating envelope of the compressor

2.3.2 Data analysis

First of all, we looked at the comparison between the theoretical mass flow rate calculated from the heat transfer in the evaporator $\dot{m}_{r,e}$ which we calculated in Section 2.2.4 and the flow rate based on the compressor model $\dot{m}_{r,c}$. There was a huge discrepancy between those mass flow rates as can be seen in Table 6. There are two ways to explain the difference in calculated data. The compressor can be damaged or the theoretical mass flow rate in the evaporator is not correct. We discuss the evaporator mass flow rate in Section 2.2.4.

We also compared the measured temperatures $T_{d,m}$ at the compressor discharge line with the ideal isentropic compressor output temperature $T_{d,die}$ and the model output temperature $T_{d,t}$. The measured temperature is below the ideal isentropic compressor temperature. Based on this measurement the compressor should be more efficient than ideal compressor. However, it is more likely that the measured temperature is incorrect due to improper sensor mounting as can be seen in Fig. 8.

	p_s [bar]	p_d [bar]	$T_{d,t}$ [°C]	$T_{d,ie}$ [°C]	$T_{d,m}$ [°C]	$\dot{m}_{r,e}$ [kg/h]	$\dot{m}_{r,c}$ [kg/h]	$\dot{m}_e/\dot{m}_c$ [−]
Exp 1	8.64	27.7	79.2	71.9	65.7	28.2	58.9	0.479
Exp 2	8.58	35.1	93.1	86.3	81.5	39.7	75.9	0.523
Exp 3	8.88	34.1	90	83.9	82.8	44.1	80.1	0.55
Exp 4	8.57	36.7	96.6	89.1	85.7	28.4	73.7	0.386
Exp 5	8.8	34	90.1	83.9	81.7	33.4	79.4	0.421
Exp 6	8.72	33.7	89.6	83.5	81.3	38.2	79.2	0.483
Exp 7	8.54	35.8	94.6	87.5	84.7	23.1	74.7	0.309
Exp 8	8.67	33.5	89.4	83.3	83	29.3	78.9	0.371
Exp 9	8.4	32.8	88.7	82.5	82.6	28.3	77.3	0.366
Exp 10	8.21	16.1	50.8	42.5	35.7	5.27	13.6	0.388
Exp 11	8.4	19.5	61.4	52.3	42.1	10.8	22.6	0.478
Exp 12	8.23	20.5	64.5	55.4	46.5	13.6	28.6	0.476
Exp 13	8.53	33.8	91.1	84	77.7	31.5	72	0.437
Exp 14	8.19	29.5	85.4	76.5	69.2	16.5	52.4	0.315
Exp 15	8.33	37	97.9	89.9	83.7	27	71.2	0.379
Exp 16	8.35	34.7	93	86	79.9	29.4	74.3	0.395
Exp 17	7.95	35.1	95.1	87.5	81.1	19.2	70.3	0.273
Exp 18	8.29	32.7	88.6	82.4	76.6	19.9	76.5	0.26
Exp 19	8.33	32.9	88.9	82.7	77.6	23.4	76.7	0.305
Exp 20	8.64	33.5	89.5	83.3	77.4	32.2	78.7	0.409
Exp 21	8.42	33.4	89.8	83.5	77.8	22.5	76.8	0.292
Exp 22	8.78	33.8	89.8	83.6	80.4	27.8	79.5	0.35

Table 6: Refrigerant mass flow

2.4 Expansion valve

An expansion valve is a crucial part of each heat pump. It has high resistance and a pressure drop occurs on it. At the input, the refrigerant is liquid, however, at the output, it is in a mixed state. The enthalpy remains constant in this process.

The expansion valve is commonly controlled by a super-heat controller. The controller makes sure the refrigerant flowing into the compressor is fully vaporized. When liquid refrigerant flows into the compressor it can result in damage to the compressor.

To ensure the vaporization of the refrigerant, its temperature has to be higher than its saturation temperature. The temperature difference between the saturation temperature T_s and the refrigerant temperature at the compressor input is called 'super-heat temperature'. We incorporated the super-heat controller into the model of the expansion valve with artificial dynamics to achieve the steady state.

2.5 Model implementation

The expansion valve model we created has six inputs, two internal variables, and three outputs. The inputs are the refrigerant enthalpy H_i, pressure p_i, mas flow rate $\dot{m}_{r,o}$, the output pressure p_o, the enthalpy at the evaporator output H_{sh} and the super-heat temperature T_{sh}. The input pressure is not used in any equation, but it is present in case the model of the expansion valve changes in the future.

The two internal variables of the model are the output flow rate $\dot{m}_{r,i}$ and the output enthalpy H_o. The output enthalpy is implemented to break an algebraic loop when AWG-DW model is put together in Section 3.1.

We were not concerned with the time dynamics of the super-heat controller, but only in the steady state refrigerant mass flow rate, for which the super-heat temperature is achieved. The heat transferred in the evaporator

$$\dot{Q}_e = (H_{sh} - H_o)\,\dot{m}_{r,o}. \tag{74}$$

is compared with the heat which would be transferred if the super-heat temperature was achieved

$$\dot{Q}^* = (H(T_s + T_{sh}, p_o) - H_o)\,\dot{m}_{r,o}. \tag{75}$$

If the theoretical heat transfer $\dot{Q}^*$ is higher than the heat transfer in the evaporator $\dot{Q}_e$, the estimated refrigerant mass flow rate is too high, and vice versa. Based on the ratio of these heat transfer rates, we can also estimate the steady state mass flow rate

$$\dot{m}^*_{r,o} = \frac{\dot{Q}^*}{\dot{Q}_e}\dot{m}_{r,o}. \tag{76}$$

Based on these principles we implemented the derivatives of the internal variables as

$$\frac{d\dot{m}_{r,o}}{dt} = \dot{m}^*_{r,o} - \dot{m}_{r,o}, \tag{77}$$

$$\frac{dH_o}{dt} = H_i - H_o. \tag{78}$$

2.6 Fan

A fan is utilized to create the airflow through AWG-DW. Based on the affinity laws published by Čermák [17], we created a model describing the relation between the rotation speed n, volumetric flow rate $\dot{V}$ and input power P_f

$$\dot{V} \approx C_1 n, \tag{79}$$

$$P_f \approx C_2 n^3, \tag{80}$$

$$P_f \approx C_2 \left(\frac{\dot{V}}{C_1} \right)^3. \tag{81}$$

The power consumption of the fans was not measured in the dataset and we did not expect the model of the fan to have a high influence on the dynamics of the whole system. We calibrated the model based on the maximum flow rate $\dot{V}_{max}$ and power consumption $P_{f,max}$ as shown in Eq. (82).

$$P_f = P_{f,max} \left(\frac{\dot{V}}{\dot{V}_{max}} \right)^3 \tag{82}$$

2.7 Dumper valve

In some operating conditions, there is a need to increase the heat transfer in the condenser while maintaining the flow rate through the evaporator. Since the airflow through the evaporator $\dot{V}_e$ and the condenser $\dot{V}_c$ is driven by the same fan, there is a need for a valve that would let some of the air flowing through the condenser escape the duct before going through the evaporator. This functionality is achieved using the dumper valve positioned after the condenser.

Since there was no reliable data for the modeling of this valve we decided to model the valve simply as a linear flow divider. Such linearity may be achieved later by a valve controller.

$$\dot{V}_e = c\dot{V}_c \qquad\qquad 0 < c \leq 1 \tag{83}$$

2.8 Electric heater

In an electric heater the temperature of the air is increased in order to increase the mass transfer in the desiccant wheel. The electric heater itself is part of the desiccant wheel assembly.

It was reported that there have been attempts to measure the air temperature between the electric heater and the desiccant wheel. Due to the short distance between those to parts the temperature sensor was placed close to the electric heater. The sensor was measuring temperatures in excess of $100°\mathrm{C}$ as it was heated by the radiation heat.

As there was no usable measurements and no significant dynamics was found, we decided to model the the electric heater as a 100 % efficient converter of the electric energy into the heat of the air

$$T_{a,o} = T_{a,i} + \frac{P_h}{\dot{V}_e \rho_a c_a}. \tag{84}$$

2.9 Desiccant wheel

2.9.1 Overview

Desiccants are materials that exhibit an affinity for water vapor. In everyday life, they can be often seen as a small bag of silica gel which absorbs humidity in the packages of various goods. They are also used in many cooling, dehumidification and enthalpy recovery applications. They can be both solid and liquid but for the purpose of this thesis, we will focus only on solid desiccants shaped into the form of a wheel.

The desiccant wheel is a rotating matrix with many channels parallel to the axis of rotation. The flow channels of the desiccant wheel are built in different shapes, namely: hexagonal, triangular and sinusoidal. The wheel rotates continuously with a constant speed of 6 to $14\,\mathrm{rev/h}$. This matrix acts as a medium for heat and mass transfer between colder process air and warmer regeneration air. The heat and mass is transferred between the desiccant and the process air. The channel of the desiccant wheel is then rotated out of the process air into the regeneration air. Heat and mass is then transferred between between the process air and the desiccant.

When the warmer regeneration air flows through a channel, the wheel heats up and discharges the water content. In the parts where the colder process air flows, the wheel cools down and receives moisture from the air.

The main functional principle of desiccants is that its relative humidity is almost independent on the temperature of the desiccant wheel. When the warmer regeneration air has lower relative humidity. Therefore, when it flows through the desiccant, the humidity is transferred to the air in order to match the relative humidity of the desiccant. Therefore absolute humidity of the desiccant decreases. In the process phase, the desiccant gains its humidity back from the cold process air which has higher relative humidity. The relative humidity of the air is always between the relative humidity of regeneration and process air.

In this section, we focus on the development of the desiccant wheel model based on the general equations of desiccants. We present two ways to develop the mathematical model: one based on the discretization of partial differential equations and the other on the finite volume method.

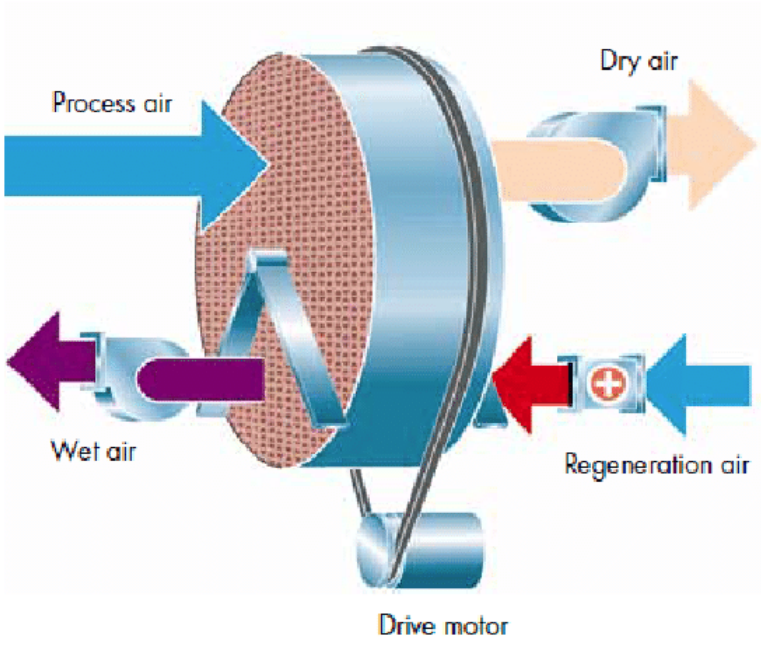

Figure 11: Drawing of Desiccant wheel [18]

2.9.2 Model description

ρ_a density of air $[\mathrm{kg\,m^{-3}}]$
ρ_d density of desiccant $[\mathrm{kg\,m^{-3}}]$
K_x gas-side mass transfer coefficient $[\mathrm{kg\,m^{-2}\,s^{-1}}]$
h air-side convective heat transfer coefficient $[\mathrm{J\,m^{-2}\,s^{-1}\,K^{-1}}]$
k_a thermal conductivity of air $[\mathrm{W\,m^{-1}\,K^{-1}}]$
k_d thermal conductivity of desiccant $[\mathrm{W\,m^{-1}\,K^{-1}}]$
D_e mass diffusion of desiccant $[\mathrm{kg\,m^{-1}\,K^{-1}}]$
d_e hydraulic diameter $d_e = 4A/P$
P channel cross section perimeter
c_{pa} specific heat of air $[\mathrm{J\,kg^{-1}\,K^{-1}}]$
c_{pd} specific heat of desiccant $[\mathrm{J\,kg^{-1}\,K^{-1}}]$
c_{psd} specific heat of desiccant matrix support material $[\mathrm{J\,kg^{-1}\,K^{-1}}]$
c_{pv} specific heat of water vapor $[\mathrm{J\,kg^{-1}\,K^{-1}}]$
c_{pw} specific heat of water $[\mathrm{J\,kg^{-1}\,K^{-1}}]$
q_{st} heat of sorption $[\mathrm{J\,kg^{-1}_{adsorbate}}]$
W desiccant adsorption mass $[\mathrm{kg_{adsorbate}/kg_{adsorbent}}]$
X_a absolute humidity ratio of the air stream $[\mathrm{kg_{water\ vapor}/kg_{dry\ air}}]$
X_d humidity ratio in equilibrium with the desiccant $[\mathrm{kg_{water\ vapor}/kg_{dry\ air}}]$
T_d temperature of desiccant $[^\circ\mathrm{C}]$
T_a temperature of air $[^\circ\mathrm{C}]$
v air flow rate speed $[\mathrm{m\,s^{-1}}]$
f desiccant mass fraction in the wall or in the matrix
n the number of the channel
m_m total mass of the matrix in the dehumidifier $2\delta\rho_m n x_w L$ [kg]
δ the thickness of desiccant [m]
L actual process channel length (desiccant wheel thickness) [m]
H_g enthalpy of air $[\mathrm{J\,kg^{-1}}]$
H_m enthalpy of desiccant matrix $[\mathrm{J\,kg^{-1}}]$
t_{proc} time period of process air [s]
t_{reg} time period of regeneration air [s]
t_{per} time period of desiccant wheel rotation $(t_{proc} + t_{reg})$ [s]

Due to the cylindrical nature of the desiccant wheel, Euler cylindrical coordinates are often used: axial direction (z), radial direction (r) and circumferential angle (ϕ) as show in Fig. 12.

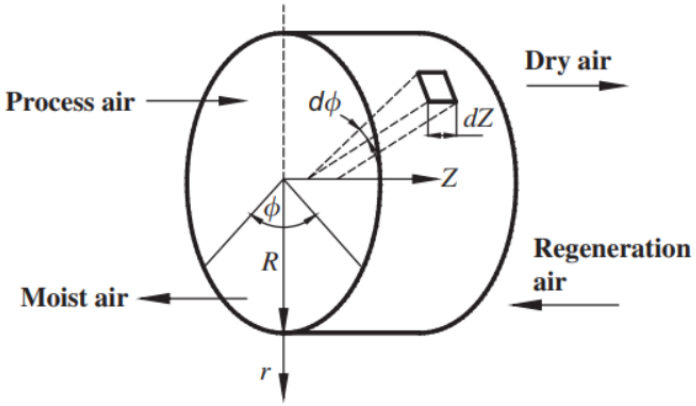

Figure 12: Coordinate system of desiccant wheel [19]

We assume the air stream is uniformly split between the channels of the desiccant matrix. This in term means that each channel located at the same angle ϕ is subject to the same input air proprieties. Therefore, those channels have identical water content and temperature independent of the distance r from the center.

There are four equations describing the mass and heat transfer between the desiccant and the air [19]. These equations describe one of the channels of the desiccant wheel in time and its length along the airflow. However, the wheel rotates at a constant speed, therefore in the steady state, the time derivative is proportional to the derivative by the angle ϕ because the wheel rotates by angle $\Delta\phi$ in time Δt and the properties of the air and desiccant at each position of the wheel does not change in the steady state.

Mass transfer of the water into air is

$$d_e \rho_a \left(\frac{\partial X_a}{\partial t} + v \frac{\partial X_a}{\partial z} \right) = K_x (X_d - X_a). \tag{85}$$

The first term on the left-hand side (LHS) of Eq. (85) is the moisture storage in the air. The second term describes the mass transfer due to the flow of air. The term on the right hand side (RHS) is the mass transfer rate of water between the air and the desiccant.

Mass transfers in the desiccant can be expressed as

$$f \delta \rho_d \left(\frac{\partial W}{\partial t} - D_e \frac{\partial^2 W}{\partial z^2} \right) = -K_x (X_d - X_a). \tag{86}$$

The first term on the LHS of Eq. (86) is the moisture storage in the desiccant. The second term describes the mass gained by the diffusion in the solid desiccant.

Heat transfer to the air can be written as follows

$$d_e \rho_a \left(c_{pa} + X_a c_{pv} \right) \left(\frac{\partial T_a}{\partial t} + v \frac{\partial T_a}{\partial z} \right) - k_a d_e \frac{\partial^2 T_a}{\partial z^2} = h(T_d - T_a) + c_{pv} K_x (X_d - X_a)(T_d - T_a). \tag{87}$$

LHS is analogical to Eqs. (85) and (86). The terms on the LHS are: the heat stored as the temperature difference, heat transferred by the airflow and the heat transfer caused by diffusion. On the RHS there is the heat transferred due to the temperature difference and the cooling of the water

Heat transfers to desiccant wheel is given by

$$\begin{aligned} d_e c_m \rho_d \frac{\partial T_d}{\partial t} - k_d d_e \frac{\partial^2 T_d}{\partial z^2} &= -h(T_d - T_a) - q_{st} K_x (X_d - X_a) - c_{pv} K_x (X_d - X_a)(T_d - T_a) \\ c_m &= \left(f(c_{pd} + W c_{pw}) + (1 - f) c_{psp} \right). \end{aligned} \tag{88}$$

The LHS is similar to the previous equation. The RHS is also quite similar to the previous equation, except for the second term is the heat of sorption which is the heat the desiccant wheel gains as it absorbs the water vapor. The heat of sorption is changing with the amount of absorbed water in the absorbent (desiccant). Pesaran [20] described the following relations: for RD (regular density) gel

$$\begin{aligned} q_{st} &= -12400W + 3500, \quad W \leq 0.05 \\ q_{st} &= -1400W + 2950, \quad W > 0.05 \end{aligned} \tag{89}$$

and for ID (intermediate density) silica gel

$$\begin{aligned} q_{st} &= -300W + 2095, \quad W \leq 0.15 \\ q_{st} &= -2050W, \quad W > 0.15 \end{aligned} \tag{90}$$

2.9.2.1 Constrains

Equations that we use in the Section 2.9.2 describe the development of a single channel in the desiccant matrix. This channel is rotating with the matrix at a constant speed. The position of the channel is determined by the time of rotation and its initial position. The air properties are determined by the position of the channel. This in terms means that the time can be converted into the position of the channel and vice versa. The boundary conditions describing the properties of the input air for each rotation of the desiccant wheel is

$$\begin{aligned}
T_a(0,t) &= T_{proc\ air} && 0 \le t < t_{proc}, && \\
X_a(0,t) &= X_{proc\ air} && 0 \le t < t_{proc}, && \\
v(z,t) &= v_{proc\ air} && 0 \le t < t_{proc} && 0 \le z \le L, \\
T_a(L,t) &= T_{reg\ air} && t_{proc} \le t < t_{per}, && \\
X_a(L,t) &= X_{reg\ air} && t_{proc} \le t < t_{per}, && \\
v(z,t) &= -v_{reg\ air} && t_{proc} \le t < t_{per} && 0 \le z \le L.
\end{aligned} \tag{91}$$

An important note is that we are modeling a desiccant wheel with counter flow of the process and regeneration air. Therefore, the air velocity in the regeneration part of the wheel is considered negative. The steady state of the desiccant wheel can be expressed by the periodicity in time given by

$$\begin{aligned}
T_a(t,z) &= T_a(t+t_{per},z) && 0 \le t < t_{per} && 0 \le z \le L, \\
X_a(t,z) &= X_a(t+t_{per},z) && 0 \le t < t_{per} && 0 \le z \le L, \\
T_d(t,z) &= T_d(t+t_{per},z) && 0 \le t < t_{per} && 0 \le z \le L, \\
W(t,z) &= W(t+t_{per},z) && 0 \le t < t_{per} && 0 \le z \le L.
\end{aligned} \tag{92}$$

2.9.2.2 Desiccant boundary layer model

The equilibrium between the air and desiccant defines the relation between the amount of water in the desiccant in the steady state and the properties of surrounding air.

One of the equations used to describe this relationship is based on the relative humidity of the thin air layer RH_d, separation factor R and maximum water contend of the absorbent W_{max}

$$\frac{W}{W_{max}} = \frac{\mathrm{RH}_d}{R + (1-R)\mathrm{RH}_d}. \tag{93}$$

Pesaran [20] obtained the equilibrium relative humidity on the surface of RD (regular density) silica gel by fitting fourth-degree polynomial to data provided by manufacturer

$$\mathrm{RH}_d = 0.0078 - 0.0575W + 24.1W^2 - 124W^3 + 204W^4. \tag{94}$$

If the desiccant is not in the equilibrium with the surrounding air it is assumed that there is an infinitely thin layer of air at the surface of the desiccant. This thin layer always has the same temperature and relative humidity as the desiccant. Its absolute humidity can be calculated using equations described in Section 1.2. The heat and mass exchange is done between this thin air layer and the surrounding air by Fick's laws of diffusion.

2.9.2.3 Output air properties

It is often assumed the air is uniformly split between the channels of the desiccant matrix and it is perfectly mixed after coming through the desiccant wheel. Therefore the output air properties are the mean values over the respective time period

$$
\begin{aligned}
T_{Proc_{Out}} &= \frac{1}{t_{proc}} \int_0^{t_{proc}} T_a(t, L)dt, \\
X_{Proc_{Out}} &= \frac{1}{t_{proc}} \int_0^{t_{proc}} X_a(t, L)dt, \\
T_{Reg_{Out}} &= \frac{1}{t_{reg}} \int_{t_{proc}}^{t_{per}} T_a(t, 0)dt, \\
X_{Reg_{Out}} &= \frac{1}{t_{reg}} \int_{t_{proc}}^{t_{per}} X_a(t, 0)dt.
\end{aligned}
\tag{95}
$$

2.9.3 Gas-side resistance method (GSR)

Charoensupaya and Worek [21] derived a relatively simple unidirectional model of dehumidifier based on the following assumptions:

1. The desiccant consist of identical, uniformly distributed tubes.
2. All the channels are adiabatic and impermeable.
3. There is no heat conduction and molecular diffusion in the desiccant coating in the axial direction (z) .
4. Heat conduction and molecular diffusion in the air in the axial direction (z) is negligible .
5. There are no gradients of temperature or moisture content in the radial direction (Heat conduction and molecular diffusion are infinitely large).
6. The inlet air conditions are uniform radially but can be time variant.
7. The thermodynamic properties of the dry air and the properties of the desiccant wheel materials are constant.
8. The transfer coefficients between the air stream and desiccant for heat and mass transfer are constant for the process and regeneration air.
9. The pressure and velocity losses of the air stream in the axial direction are neglected.
10. The centrifugal force in the desiccant wheel is neglected.

Based on the assumptions 3 and 4, the dynamics of the solid side of the desiccant wheel are neglected. It also simplifies the equations as there are no second derivatives. This model neglects the dynamics within the desiccant wheel itself. Hai-Yun Xing [22] also omit the time derivatives of the air temperature and humidity way smaller than the derivative along the flow direction. The resulting equations

$$d_e \rho_a v \frac{\partial X_a}{\partial z} = K_x(X_d - X_a), \tag{96}$$

$$f \delta \rho_d \left(\frac{\partial W}{\partial t} \right) = -K_x(X_d - X_a), \tag{97}$$

$$d_e \rho_a \left(c_{pa} + X_a c_{pv}\right) v \frac{\partial T_a}{\partial z} = h(T_d - T_a) + q_{st} K_x(X_d - X_a) + c_{pv} K_x(X_d - X_a)(T_d - T_a), \tag{98}$$

$$
\begin{aligned}
d_e c_m \rho_d \frac{\partial T_d}{\partial t} &= -h(T_d - T_a) - q_{st} K_x(X_d - X_a) - c_{pv} K_x(X_d - X_a)(T_d - T_a), \\
c_m &= \left(f(c_{pd} + W c_{pw}) + (1 - f)c_{psp}\right).
\end{aligned}
\tag{99}
$$

2.9.4 Numerical solution

The partial differential equations describing the desiccant wheel dynamics are non-linear, especially the function for absolute air humidity in equilibrium with the desiccant (Section 2.9.2.2). Kang [23] and Lee [24] managed to create an analytical solution for the desiccant wheel using certain assumptions. There is no general solution for the desiccant wheel, and generally the numerical solutions tend to achieve better results.

2.9.4.1 Euler method

Euler methods are first order methods for discretization of the differential equations. If the derivative of the system's states is constant for the duration of the step size then the method is absolutely accurate. There exist two versions of this method: forward (Eq. (100)) and backward (Eq. (101)), sometimes they are called explicit and implicit. The main advantage of this method is its simplicity and which allows fast calculation. The main disadvantage is the global error of this discretization method which is proportional to step size h.

$$x(n+1) = x(n) + hf\left(x(n), u(n)\right) \tag{100}$$

$$x(n+1) = x(n) + hf\left(x(n+1), u(n+1)\right) \tag{101}$$

2.9.4.2 Runge–Kutta fourth-order method

The Runge-Kutta method is based on the same theoretical background as the Euler method, the Taylor polynomial. However, the Runge-Kutta method is more complex and therefore achieves an global error rate proportional to step size to the power of four (h^4).

$$\begin{aligned}
k_{1,n} &= f(x(n), u(n)) \\
k_{2,n} &= f(x(n) + h/2 \cdot k_{1,n}, u(n)) \\
k_{3,n} &= f(x(n) + h/2 \cdot k_{2,n}, u(n)) \\
k_{4,n} &= f(x(n) + h \cdot k_{3,n}, u(n)) \\
x(n+1) &= x(n) + h/6 \cdot (k_{1,n} + 2\,k_{2,n} + 2\,k_{3,n} + k_{4,n})
\end{aligned} \tag{102}$$

2.9.4.3 Hermite-Simpson collocation method

Forward Euler method as well as the Runge–Kutta method are explicit. Ge [19] achieved better result using implicit methods rather than explicit when solving the desiccant wheel equations. The idea behind this method is that the states are approximated by a cubic function.

$$\begin{aligned}
k_{1,n} &= f(x(n), u(n)) \\
k_{2,n} &= f(x(n+1), u(n+1)) \\
x_{c,n} &= (x(n) + x(n+1))/2 + h \cdot (k_{1,n} - k_{2,n})/8 \\
k_{c,n} &= f(x_{c,n}, (u(n) + u(n+1))/2) \\
h \cdot k_{c,n} &+ 3 \cdot (x(n) - x(n+1))/2 + h \cdot (k_{1,n} + k_{2,n})/4 = 0
\end{aligned} \tag{103}$$

2.9.5 System discretization using backward euler method

While developing the model the desiccant wheel, we tried many methods of discretization of the model. One of them was the backward Euler, because it was reported [19] it achieves better stability and accuracy compared to the forward Euler method. If we apply the backward Euler method to Eqs. (96) to (99), we get a set of equations, which must be satisfied in the steady state.

$$d_e \rho_a v \frac{X_a(z,t) - X_a(z-\Delta z,t)}{\Delta z} = K_x(X_d(z,t) - X_a(z,t)) \tag{104}$$

$$f\delta\rho_d \left(\frac{W(z,t) - W(z,t-\Delta t)}{\Delta t} \right) = -K_x(X_d(z,t) - X_a(z,t)) \tag{105}$$

$$\begin{aligned} d_e \rho_a \left(c_{pa} + X_a c_{pv}\right) v \frac{T_a(z,t) - T_a(z-\Delta z,t)}{\Delta z} =& h(T_d(z,t) - T_a(z,t)) + q_{st} K_x(X_d(z,t) - X_a(z,t)) \\ &+ c_{pv} K_x(X_d(z,t) - X_a(z,t))(T_d(z,t) - T_a(z,t)) \end{aligned} \tag{106}$$

$$\begin{aligned} d_e c_m(z,t) \rho_d \frac{T_d(z,t) - T_d(z,t-\Delta t)}{\Delta t} =& -h(T_d(z,t) - T_a(z,t)) - q_{st} K_x(X_d(z,t) - X_a(z,t)) \\ &- c_{pv} K_x(X_d(z,t) - X_a(z,t))(T_d(z,t) - T_a(z,t)) \\ c_m(z,t) =& (f(c_{pd} + W(z,t) c_{pw}) + (1-f) c_{psp}) \end{aligned} \tag{107}$$

2.9.6 Finite volume method

The idea behind the finite volume method is that the desiccant wheel is split into a certain number of segments each taking up angle φ. In time Δt the wheel rotates by $\Delta\varphi$, a part of this segment is rotated out of the volume element and only $(\frac{\varphi-\Delta\varphi}{\varphi})$ of the original volume is left while a part of the previous element $(\frac{\Delta\varphi}{\varphi})$ is rotated into it. The air in each volume element is then perfectly mixed. In the time Δt, the heat and mass is exchanged between the desiccant and the air.

First, we derive the change of desiccant adsorption mass ΔW_k

$$\begin{aligned} \Delta W_k &= \frac{W_k(\varphi - \Delta\varphi) + W_{k-1}\Delta\varphi}{\varphi} + \frac{\partial W}{\partial t}\Delta t - W_k, \\ \Delta W_k &= \frac{-\omega\Delta t W_k + \omega\Delta t W_{k-1}}{\varphi} + \frac{\partial W}{\partial t}\Delta t, \\ \frac{\Delta W_k}{\Delta t} &= \omega\frac{-W_k + W_{k-1}}{\varphi} + \frac{\partial W}{\partial t}, \\ \frac{\Delta W_k}{\Delta t} &= \omega\frac{-W_k + W_{k-1}}{\varphi} + \frac{-K_x(X_{d_k} - X_{a_k})}{f\delta\rho_d}. \end{aligned} \tag{108}$$

By making the time interval Δt infinitely small $\frac{\Delta W_k}{\Delta t}$ becomes $\frac{\partial W_k}{\partial t}$. In the steady state, the amount of water in the desiccant does not change, therefore the time derivative is zero

$$\begin{aligned} \frac{\partial W_k}{\partial t} &= \omega\frac{-W_k + W_{k-1}}{\varphi} + \frac{-K_x(X_{d_k} - X_{a_k})}{f\delta\rho_d}, \\ 0 &= \omega\frac{-W_k + W_{k-1}}{\varphi} + \frac{-K_x(X_{d_k} - X_{a_k})}{f\delta\rho_d}, \\ \omega\frac{W_k - W_{k-1}}{\varphi} &= \frac{-K_x(X_{d_k} - X_{a_k})}{f\delta\rho_d}. \end{aligned} \tag{109}$$

A similar approach can be used to derive the equations for the enthalpy of the desiccant matrix which is determined by

$$H_m = (f(c_{pd} + Wc_{pw}) + (1-f)c_{psp}) = c_m(W)T. \tag{110}$$

If we neglect the density difference due to the water content then we get the equations for temperature from mixing of the enhlapies:

$$\begin{aligned} \Delta H_k &= \frac{H_k(\varphi - \Delta\varphi) + H_{k-1}\Delta\varphi}{\varphi} + \frac{\partial H}{\partial t}\Delta t - H_k \\ \Delta H_k &= \frac{-\omega\Delta t H_k + \omega\Delta t H_{k-1}}{\varphi} + \frac{\partial H}{\partial t}\Delta t \\ \frac{\Delta H_k}{\Delta t} &= \omega\frac{-H_k + H_{k-1}}{\varphi} + \frac{\partial H}{\partial t} \\ \frac{\Delta H_k}{\Delta t} &= \omega\frac{-(c_d T_k + c_w W_k T_k) + (c_d T_{k-1} + c_w W_{k-1} T_{k-1})}{\varphi} + \frac{\partial H}{\partial t} \end{aligned} \tag{111}$$

Neglecting the heat capacity change of the desiccant matrix (c_m) due to the different water content, we get .

$$\frac{\Delta H_k}{\Delta t} = \omega(c_d + c_w W_k)\frac{-T_k + T_{k-1}}{\varphi} + \frac{\partial H}{\partial t}. \tag{112}$$

Using this approximation we derive the condition for the steady state solution by setting the time derivative of the enthalpy of the k-th element to zero

$$\omega\frac{T_k - T_{k-1}}{\varphi} = \frac{1}{d_e c_m \rho_d}\left(-h(T_{d_k} - T_{a_k}) - q_{st}K_x(X_{d_k} - X_{a_k}) - c_{pv}K_x(X_{d_k} - X_{a_k})(T_{d_k} - T_{a_k})\right). \tag{113}$$

With the finite volume method, we achieved the same equations as we get by discretizing Eqs. (97) and (99) using the backward Euler method, where the time derivatives of the air temperature and humidity.

2.9.7 Model implementation

Unlike the other components of AWG-DW, the desiccant wheel has a lot of internal variables. The wheel is split into two parts: the process air and the regeneration air part. In each of those parts, the wheel is discretized in two dimensions along the rotation of the wheel (time of rotation) and the flow of the air. In each of those discretized points, there is the temperature and the humidity ratio. We also attempted to simplify the model by not discretizing along the flow axis . However, this model was able to describe the data with reasonable accuracy.

Due to the nature of the system, we had to make the discretization in relatively fine steps. For the desiccant to start releasing water into regeneration air, the desiccant has to heat up first, because the absolute humidity of the thin air film in equilibrium with the desiccant is highly dependent on the temperature of the desiccant.

In our search for the system parameters, we had two options to choose from. We could either create a separate steady state finder that would find the steady state of the desiccant wheel and the resulting output for a given set of parameters. The optimal parameters will be then found using this steady state finder.

The other option was to let the algorithm which will be searching the best set of parameters to find the steady state internal variables of the desiccant wheel. We used CasADi [25] in our attempts to implement this method. However, we were not able to implement this model successfully. One of the problems we encountered in the process was the sheer amount of internal variables. The already

high number of internal variables was multiplied by the number of experiments we used to find the parameters. The discretization had to be quite coarse otherwise the program would run out of system memory.

In the steady state finder, we could either use gradient decent method or simulate the desiccant wheel. We decided to simulate the wheel and we could either simulate the whole desiccant wheel at once (motivated by the finite volume method) or we could simulate just one of the channels of the desiccant wheel rotating within it (motivated by the discretization of the partial differential equations).No matter the way, the steady state should be always the same.

After some trials and errors, we used the Runge–Kutta fourth-order method to discretize the dynamics along the flow of the air as well as for the dynamics along the rotation of the wheel (time). We later replaced the Runge–Kutta method along the rotation of the wheel by the *ode23* Matlab function because it was faster, probably due to the way it is implemented and it also achieved a better result with fewer steps.

We simulated only a single channel rotating in the matrix, because we used an explicit method. It made little sense to simulate the whole wheel at once, as it would be significantly slower.

The simulation runs until the variables of the desiccant channel at the beginning of the rotation match with the one at the end of the rotation of the desiccant wheel, i.e. steady state is found.

2.9.7.1 Polynomial fit of model output

Another challenge was raised when the model was supposed to be integrated in AWG-DW model. At first, we tried to implement the dynamic model, however, high number of internal variables extremely decreased the speed of numerical algorithms. For those reasons, we tried to pre-compute the results model and then use an interpolation function. However, CasADi [25] inside the NLCM [6] toolbox does not support the interpolation function. Therefore, we decided to interpolate the pre-calculated data with fourth degree polynomial over four variables totaling 256 polynomial coefficients. The method to calculate these coefficients was introduced by Wahl [26, 27] and implemented by the supervisor of this thesis. We were concerned about over-fitting the polynomial, therefore we generated about fifty thousand samples by the model and then interpolated them to gain over million samples. We also contained the first derivatives by the outside air properties. With increasing outside air temperature, the regeneration air output temperature has to increase and the absolute humidity should decrease. With increasing outside air absolute humidity, the regeneration air output temperature has to decrease and the absolute humidity should increase as can be seen in Fig. 13.

The model used in the simulation of AWG-DW is this polynomial fit. It has six inputs, six outputs and no internal states. The input, as well as the output, are the properties of the regeneration and process air, namely: temperature T, absolute humidity X and volumetric flow rate $\dot{V}$. The process air volumetric flow rate was fixed to $400\,\mathrm{m^3\,h^{-1}}$ in all calculations and experiments of AWG-DW as well.

The output regeneration air humidity and temperature are computed using the polynomial interpolation. The conservation of energy and mass principles are used to determine the output properties of the process air

$$\dot{m}_w = \Delta X_{a,p} \dot{V}_{a,p} \rho_a = \Delta X_{a,r} \dot{V}_{a,r} \rho_a, \tag{114}$$

$$\dot{Q} = \Delta H_{a,p} \dot{V}_{a,p} \rho_a = \Delta H_{a,r} \dot{V}_{a,r} \rho_a. \tag{115}$$

2.9.8 Model calibration and data analysis

The calibration was focused on the accuracy of the temperature and absolute humidity of the output regeneration air. More emphasis was put on the humidity accuracy. The measured values in Table 7 are denoted with '*m*' subscription and the theoretical ones based on the model have subscription '*t*'. The root mean square error of humidity was $1.3\,\mathrm{g\,kg^{-1}}$ and of the temperature was $1.9\,^{\circ}\mathrm{C}$.

In Section 2.10, we discussed the possibility of water condensation in the heat recovery unit. However, the humidity we consider to be the output of the desiccant wheel is measured at the input of the evaporator and there is no humidity sensor between the desiccant wheel and the heat recovery unit. Therefore, there is a possibility the desiccant wheel is calibrated on incorrect data.

	X_p [g/kg]	T_p [°C]	X_r [g/kg]	T_r [°C]	$\dot{V}_r$ [m^3/h]	$\dot{V}_p$ [m^3/h]	$X_{r_o,m}$ [g/kg]	$X_{r_o,t}$ [g/kg]	$T_{r_o,m}$ [°C]	$T_{r_o,t}$ [°C]
Exp 1	5	15.3	5	89.2	120	400	13.3	11.5	48.4	44.5
Exp 2	7.5	16.5	7.5	89.5	120	400	16.4	15.7	45.9	42.9
Exp 3	10	21.2	10	90.3	120	400	19.1	19.2	46.2	45.2
Exp 4	5	26.1	5	89.6	120	400	13.2	10.7	51.1	51.9
Exp 5	7.5	26.6	7.5	89.2	120	400	15.8	14.7	48.5	50.2
Exp 6	10	25.5	10	84.6	120	400	17.1	17.8	46.5	46.5
Exp 7	5	35.5	5	84.4	119	400	12	9.24	57.8	55.8
Exp 8	7.5	36.3	7.5	89.2	115	400	15.2	13.4	55.8	56.1
Exp 9	10	35.4	10	90.6	97.3	400	16.8	17.6	50.5	51.8
Exp 10	5	13.9	5	23.7	113	400	5.76	5.56	20.3	16.9
Exp 11	7.5	15.1	7.5	31.3	120	400	7.9	8.89	23.1	20.3
Exp 12	7.5	15.2	7.5	34.2	120	400	8.33	9.14	23.5	21.3
Exp 13	10	19.4	10	65.3	120	400	14.4	15.8	34.7	34.6
Exp 14	5	24.8	5	55.4	120	400	9.06	7.53	37	37.1
Exp 15	7.5	24.9	7.5	71.7	120	400	12.2	12.7	42.4	42.4
Exp 16	10	25.5	10	65.3	120	400	13.6	15	39.7	39.4
Exp 17	5	35.7	5	64.2	120	400	9.23	7.38	49.6	47.6
Exp 18	7.5	35.4	7.5	58	120	400	10.9	9.92	45.5	44.3
Exp 19	10	35.2	10	57.8	115	400	12.8	12.9	44.9	43.3
Exp 20	10	25.4	10	70.7	120	400	15.1	15.8	42.7	41.3
Exp 21	7.5	34	7.5	69.2	120	400	12.1	11.4	49.5	47.6
Exp 22	10	35.7	10	71.3	120	400	14.5	14.7	51.4	48.8

Table 7: Desiccant wheel calibration results

In Fig. 13 we can see the regeneration air output temperature and humidity for regeneration air flow rate $120\,\mathrm{m^3\,h^{-1}}$, process air flow rate $400\,\mathrm{m^3\,h^{-1}}$ and regeneration input air temperature $90\,^{\circ}\mathrm{C}$. The absolute humidity of both airflows is the same at their respective inputs. The output humidity increases with lower temperature and higher absolute humidity of the process (outside) air, because it means higher outside air relative humidity. However, the output temperature lowers with higher absolute humidity of the outside air because the heat of sorption is mostly transferred from the warmer regeneration air to the colder process air (through the desiccant wheel).

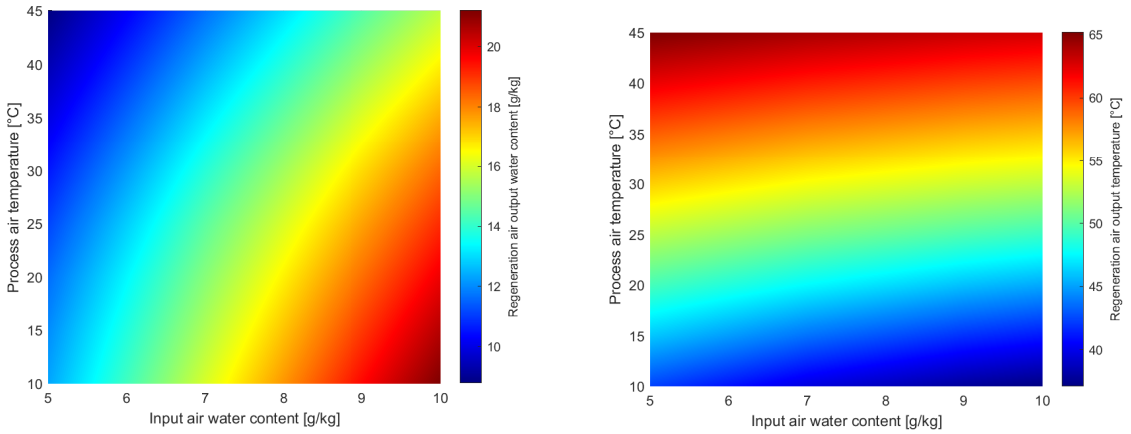

(a) Regeneration air output water content

(b) Regeneration air output temperature

Figure 13: Model regeneration air output properties for regeneration air input temperature $90\,^{\circ}\mathrm{C}$

Interesting phenomenon can be seen in Fig. 14. We can see that there is an optimal regeneration air flow rate which maximizes the output air humidity. If the flow rate is too high then the added humidity dilutes into the air. On the other hand, if the flow rate is too low the desiccant does not heat up properly and therefore does not transfer water into the air. However, there is no such extreme for the output temperature, The regeneration air output temperature is at its maximum, when the flow rate and the input temperature is maximized.

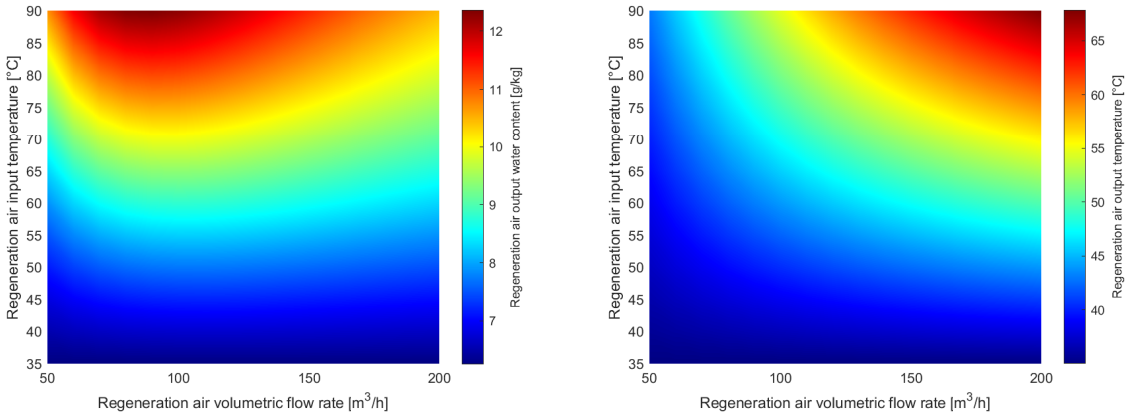

(a) Regeneration air output water content

(b) Regeneration air output temperature

Figure 14: Model regeneration air output properties for input process air temperature $35\,^{\circ}\mathrm{C}$ and humidity $6\,\mathrm{g\,kg^{-1}}$

In Fig. 15 is the visualization of the steady state temperature and air in the desiccant wheel as well as in the air. The regeneration air input temperature is $90\,^{\circ}\mathrm{C}$, the process air input temperature is $35\,^{\circ}\mathrm{C}$, the absolute humidity of both air streams is $6\,\mathrm{g\,kg^{-1}}$ and the volumetric flow rate of regeneration air was $120\,\mathrm{m^3\,h^{-1}}$.

The desiccant wheel is split into the process part and the regeneration part in 3:1 ratio. This division is marked by a vertical line at $3\pi/2$ angle of rotation. The direction of the flowing air is visualized with arrows. There are some interesting phenomenons to be observed. The water transfer rate is actually the highest right at the beginning of process air region. The warm desiccant, whose boundary layer has high absolute humidity, transfers a lot of humidity into the fresh process air. This

phenomenon is short lived, because the desiccant quickly cools down thus the absolute humidity of the boundary layer air is lowered and it can gain humidity from the process air.

It is important to note that the temperature and humidity gradient in the desiccant along the length of the channel are relatively high. It can be caused by the neglected mass diffusion and heat conduction within the desiccant.

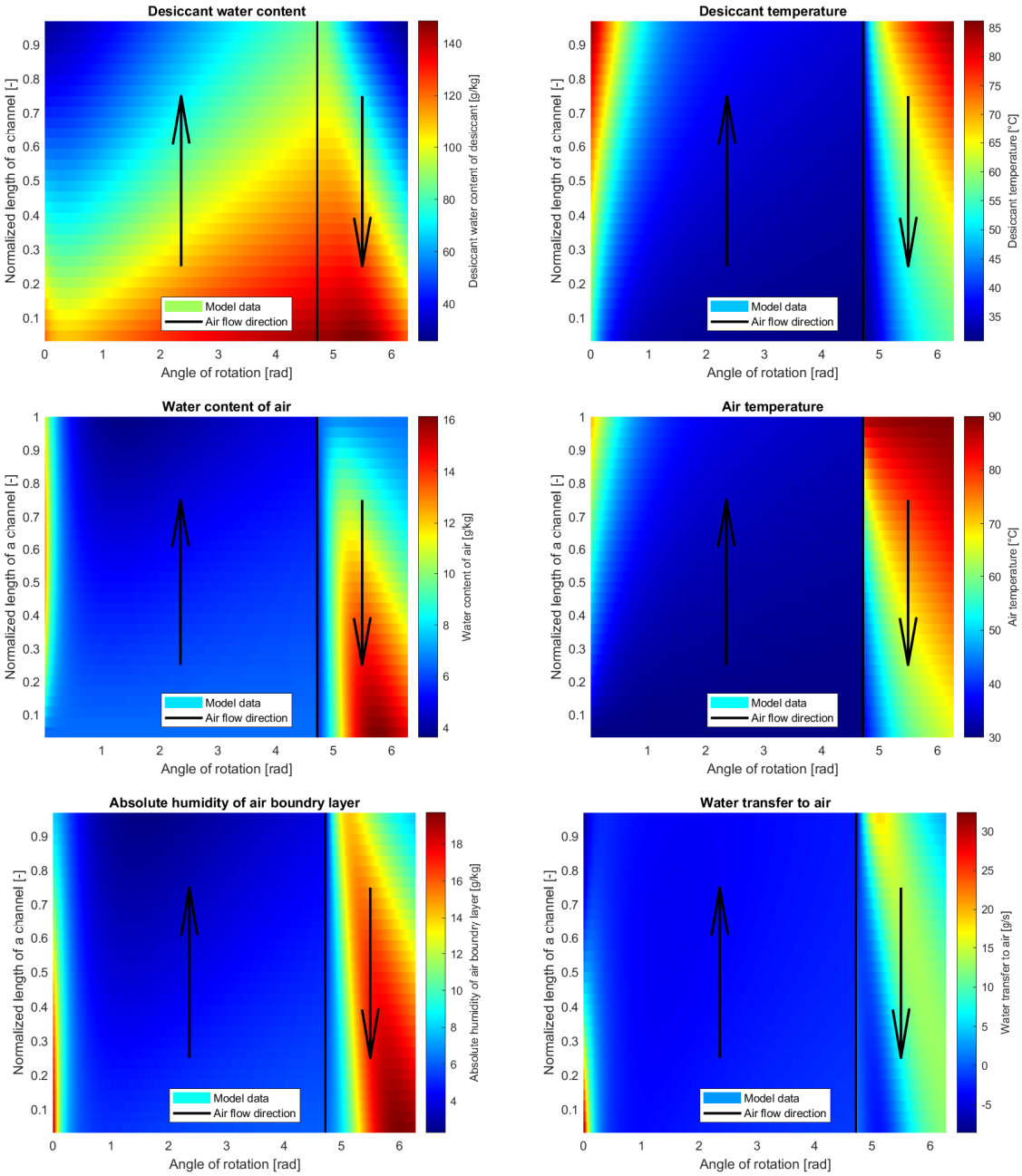

Figure 15: The modeled internal properties of air and desiccant

2.10 Heat recovery unit

$T_{a1,i}$	temperature of the primary air coming from the desiccant wheel $[^\circ\mathrm{C}]$
$T_{a2,i}$	temperature of the secondary air coming from the evaporator $[^\circ\mathrm{C}]$
X_{a1}	humidity of the air coming from the desiccant wheel $\left[\mathrm{kg_{water}\,kg^{-1}_{dry\,air}}\right]$
X_{a2}	humidity of the air coming from the evaporator $\left[\mathrm{kg_{water}\,kg^{-1}_{dry\,air}}\right]$
$\dot{V}_{a1}$	volumetric flow rate of the air coming from the desiccant wheel $\left[\mathrm{kg_{water}\,kg^{-1}_{dryair}}\right]$
$\dot{V}_{a2}$	volumetric flow rate of the air coming from the evaporator $\left[\mathrm{m^3\,s^{-1}}\right]$
c_{a1}	specific heat of air coming from the desiccant wheel $\left[\mathrm{J\,kg^{-1}\,K^{-1}}\right]$
c_{a2}	specific heat of air coming from the evaporator $\left[\mathrm{J\,kg^{-1}\,K^{-1}}\right]$
k	heat transfer coefficient $\left[\mathrm{J\,m^{-2}\,s^{-1}\,K^{-1}}\right]$
ρ_a	density of the air $\left[\mathrm{kg\,m^{-3}}\right]$

The heat recovery unit, also known as recuperator, is a counter flow heat heat exchanger. In AWG-DW, the warm air from the desiccant wheel cools down while the air coming from the evaporator heats up. The heat transfer for in the recuperator is calculated the same way as in Eq. (12). There are two air stream. In this description, we decided to name the air coming from the desiccant wheel the primary air. The air coming from the evaporator is then called the secondary air.

$$\begin{aligned}\dot{V}_{a1}\,c_{a1}\,\rho_a\,\frac{\partial}{\partial x}T_{a1}\left(x\right) &= -k\,\left(T_{a1}\left(x\right)-T_{a2}\left(x\right)\right)\\ \dot{V}_{a2}\,c_{a2}\,\rho_a\,\frac{\partial}{\partial x}T_{a2}\left(x\right) &= -k\,\left(T_{a1}\left(x\right)-T_{a2}\left(x\right)\right)\end{aligned} \tag{116}$$

Solving Eq. (116) with normalized length of the recuperator $d = 1$ and boundary conditions: input refrigerant temperature $T_{a2}(d) = T_{a2,i}$ and the air temperature $T_{a1}(0) = T_{a1,i}$ gives us the outlet temperatures of the air and the refrigerant

$$T_{a1,o} = T_{\mathrm{a2,i}} + \frac{\left(T_{\mathrm{a1,i}} - T_{\mathrm{a2,i}}\right)\,\left(V_{\mathrm{a1}}\,c_{\mathrm{a1}} - \dot{V}_{\mathrm{a2}}\,c_{\mathrm{a2}}\right)}{\dot{V}_{\mathrm{a1}}\,c_{\mathrm{a1}} - \dot{V}_{\mathrm{a2}}\,c_{\mathrm{a2}}\,\mathrm{e}^{-\frac{k\,(V_{\mathrm{a1}}\,c_{\mathrm{a1}} - V_{\mathrm{a2}}\,c_{\mathrm{a2}})}{V_{\mathrm{a1}}\,V_{\mathrm{a2}}\,c_{\mathrm{a1}}\,c_{\mathrm{a2}}\,\rho_a}}}, \tag{117}$$

$$T_{a2,o} = T_{\mathrm{a1,i}} + \frac{\left(T_{\mathrm{a1,i}} - T_{\mathrm{a2,i}}\right)\,\left(\dot{V}_{\mathrm{a1}}\,c_{\mathrm{a1}} - \dot{V}_{\mathrm{a2}}\,c_{\mathrm{a2}}\right)}{\dot{V}_{\mathrm{a2}}\,c_{\mathrm{a2}} - \dot{V}_{\mathrm{a1}}\,c_{\mathrm{a1}}\,\mathrm{e}^{\frac{k\,(\dot{V}_{\mathrm{a1}}\,c_{\mathrm{a1}} - \dot{V}_{\mathrm{a2}}\,c_{\mathrm{a2}})}{\dot{V}_{\mathrm{a1}}\,V_{\mathrm{a2}}\,c_{\mathrm{a1}}\,c_{\mathrm{a2}}\,\rho_a}}}. \tag{118}$$

2.10.1 Data analysis and model calibration

The model itself has six inputs: the temperature,humidity and volumetric flow rate of primary and secondary airflow at the inlet of the heat recovery unit. The model

The model was calibrated to minimize the error of the primary air going into the evaporator. The measured values are denoted with '*m*' subscription and the theoretically calculated ones have subscription '*t*'. The temperature error of the secondary air was not taken into the account. In the calibration results (Table 8), the root mean square error of the temperature of the air going into the evaporator was $1.9°\mathrm{C}$. However, the measured temperature of the secondary air is always higher than the theoretical ones.

	$T_{a1,i}$ [°C]	$T_{a2,i}$ [°C]	X_{a1} [g/kg]	X_{a2} [g/kg]	$\dot{V}_a$ [m^3/h]	$T_{a1,o,m}$ [°C]	$T_{a1,o,t}$ [°C]	$T_{a1,o,d}$ [°C]	$T_{a2,o,m}$ [°C]	$T_{a2,o,t}$ [°C]
Exp 1	48.4	6.72	13.3	5.88	120	20	20.4	18.4	39	35.1
Exp 2	45.9	8.09	16.4	6.41	120	23	20.6	21.7	38.3	33.8
Exp 3	46.2	10.2	19.1	7.38	120	25.4	22.2	24.1	39.4	34.7
Exp 4	51.1	10.4	13.2	7.23	120	22.3	23.7	18.2	42.6	38.1
Exp 5	48.5	11.2	15.8	7.68	120	24.1	23.5	21.1	41.6	36.6
Exp 6	46.5	10.1	17.1	7.26	120	24.2	22.2	22.4	39.4	34.9
Exp 7	57.8	11.6	12	7.83	119	23	26.6	16.8	48	43.1
Exp 8	55.8	12.5	15.2	8.29	115	25.3	26.7	20.5	47.5	42
Exp 9	50.5	12.2	16.8	7.95	97.3	24.9	24.8	22	43.1	38.3
Exp 10	20.3	3.96	5.76	4.62	113	8.66	9.21	5.87	17.8	15.1
Exp 11	23.1	4.85	7.9	5.12	120	11.8	10.7	10.5	19.8	17.3
Exp 12	23.5	4.2	8.33	4.77	120	12.6	10.4	11.2	20.3	17.3
Exp 13	34.7	8.16	14.4	6.45	120	20.5	16.9	19.7	29.7	26.2
Exp 14	37	6.84	9.06	5.77	120	16.5	16.6	12.5	31.4	27.3
Exp 15	42.4	8.27	12.2	6.38	120	19.5	19.4	17	35.1	31.5
Exp 16	39.7	8.86	13.6	6.65	120	20.7	19	18.7	33.7	29.9
Exp 17	49.6	9.12	9.23	6.51	120	20.7	22.2	12.8	42.2	36.6
Exp 18	45.5	10.3	10.9	7.2	120	20.9	21.7	15.3	39.2	34.3
Exp 19	44.9	10.5	12.8	7.25	115	21.1	21.8	17.8	38.3	33.9
Exp 20	42.7	9.78	15.1	7.08	120	22.3	20.6	20.4	35.8	32.2
Exp 21	49.5	10.4	12.1	7.3	120	20.9	23.1	16.9	41	37
Exp 22	51.4	11.8	14.5	8.05	120	23.4	24.8	19.7	42.7	38.7

Table 8: Heat recovery unit calibration results

There are many plausible explanations for this phenomenon. We suspect that there is non-negligible condensation in the unit. The dew temperature of the primary output air is below the secondary air input, therefore the it is quite likely there is some amount of condensation in the primary air. The temperature difference between the theoretical and modeled secondary air output temperature is caused by the unaccounted latent heat of the condensation. The dew temperature at the primary air output ($T_{a1,o,d}$) is above the secondary air input temperature. Therefore, it is quite likely the water is condensing in the recuperator.

The calibrated model have efficiency 68 % with the air flow $120\,\mathrm{m^3\,h^{-1}}$, which is lower than the manufacturer specifies. The discrepancy can caused by the water condensation. Further investigation and measurements of the amount of condensing water is needed, because the air humidity between the desiccant wheel and the heat recovery unit is not measured.

The datasheet of the heat recovery unit specifies the efficiency as shown in Fig. 16. According to the manufacture's website [3],the efficiency is calculated for the primary (exhaust) air with $25°C$ and 78% RH and the secondary (supply) air with $1°C$ and 28% RH. The efficiency for the primary (exhaust) air (Fig. 16) is most likely higher because of the latent heat of water condensation. However, it is not specified how this efficiency is defined.

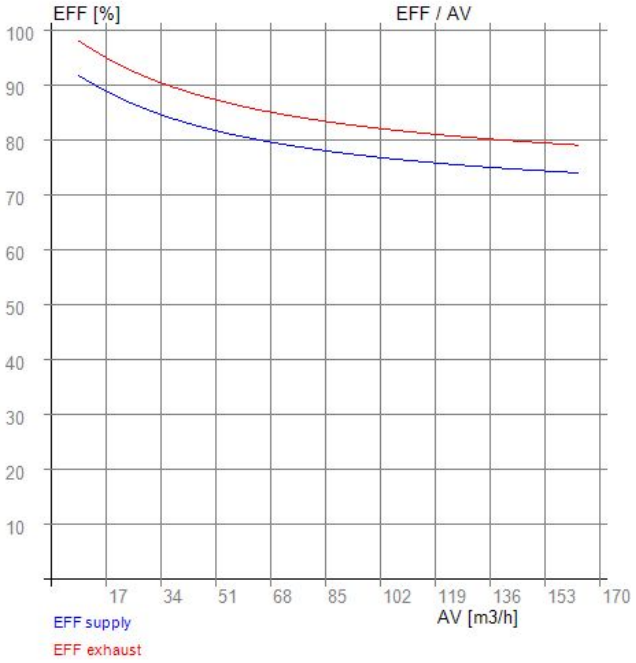

Figure 16: Efficiency map of the recuperator provided by the manufacturer

[3] rekupex.cz/hlinikove-vymeniky/9-rekuperacni-vymenik-tepla-rx-02200-rekuperator-pro-rekuperace-vzduchu.html

Chapter 3
AWG-DW model

3.1 Model implementation

As we have already mentioned, NLCM [6] and VCC [7] toolboxes were used to develop the models of the individual components connected together to create the model of whole AWG-DW model in the standardized description

$$\begin{aligned} \dot{x} &= f_c(x, u, \theta) \\ y &= g(x, u, \theta) \end{aligned} \tag{119}$$

The VCC toolbox was utilized for the properties of the refrigerant, while the NLCM toolbox for the modeling and optimization. The NLCM toolbox takes advantage of CasADi [25] toolbox for automatic differentiation and model compilation and Matlab Optimization toolbox for its numerical solvers.

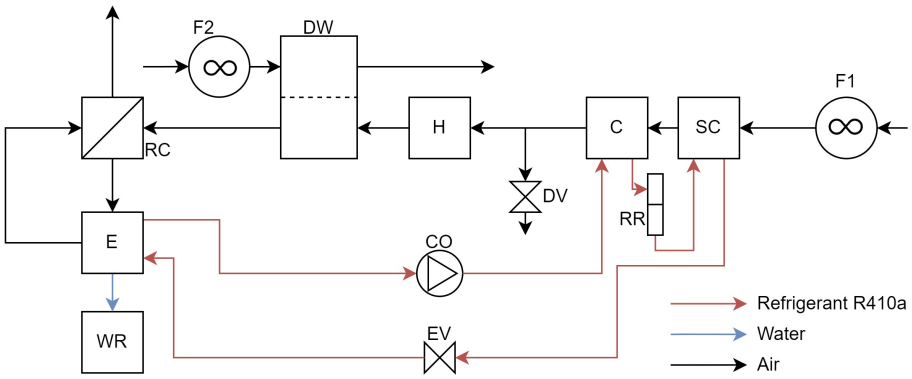

Figure 17: AWG-DW schematic

The model of AWG-DW has six variable inputs and two constant inputs. The two constant inputs are the super-heat temperature in the super-heat controller of the expansion valve and the input power of the secondary fan which pushes the air through the secondary (process) side of the desiccant wheel. The six variable inputs are as follows: the outside temperature and humidity, saturation refrigerant temperature in the evaporator, the total power consumption of AWG-DW, the position of the damper valve and the input power of the primary fan.

The power of the electric heater is calculated

$$P_{\text{electric heater}} = P_{\text{tot AWG-DW}} - P_{\text{fan 1}} - P_{\text{fan 2}} - P_{\text{comp}}. \tag{120}$$

Before the optimization, we studied the temperature and humidity in countries line Saudi Arabia, for which AWG-DW was designed. Basic statistics of the weather is shown in Fig. 18. Based on this statistics we will focus mostly on the low humidity conditions with absolute humidity of around $6\,\mathrm{g\,kg^{-1}}$.

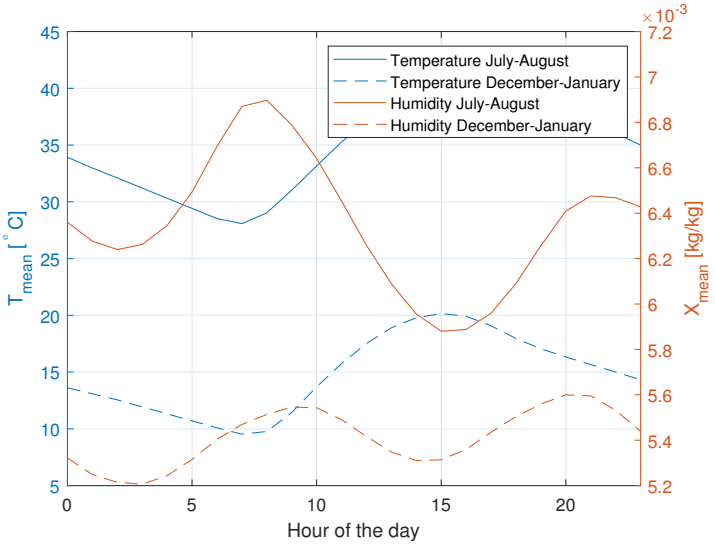

Figure 18: Mean temperature and humidity in Saudi Arabia

AWG-DW is built to be powered by a combination of solar panels and batteries. The installed solar panels have maximal power output $5.6\,\mathrm{kWp}$. The maximal measured input power of AWG-DW was $3\,\mathrm{kW}$ in high absolute humidity, low temperature conditions, the power consumption in the day should be lower than that. We expect that during the day there will be enough power to operate AWG-DW at its maximum power while also fully recharging the batteries. The main goal during this period is to maximize water production. During the night, AWG-DW is powered by its $2.2\,\mathrm{kWh}$ battery. This capacity is definitely not enough to operate AWG-DW throughout the whole night. We expect AWG-DW will run only in the morning hours when the relative humidity is highest (highest absolute humidity and lowest temperature). The main goal during the night period is to maximize water production out of the limited battery power, i.e. strive for or close to maximal water production efficiency.

An economical model predictive controller will be developed as a follow-up to this thesis. The purpose of this controller will be to increase the battery utilization efficiency based on the weather forecast, i.e. to decide whether to run at lower efficiency, but higher absolute water production, during more favorable outside conditions or not. To achieve this, we will need to know the maximum water production for given outside temperature, humidity and the total input power to AWG-DW.

Based on this analysis, we divided the optimization task into three parts. We analyzed the maximal water production for given outside conditions and total input power. In the second part, we found the maximum water production for given weather conditions and unlimited input power. Based on the principle of AWG-DW operation we knew the device is capable of wasting energy without any water production changes, therefore we imposed a secondary criteria to limit the input power. In the third part, we analyzed the maximum water production efficiency (water production per input power) for given weather conditions.

In the optimization task the either the water production or water production efficiency is maximized. The steady state is satisfied by making the states derivatives equal to zero. The inputs, outputs and state variables also have to be within their constrains

$$
\begin{aligned}
u^* = \quad & \underset{u,x}{\arg\min} \quad \dot{m}_w(x,u,\theta), \\
& s.t. \qquad\quad f_c(x,u,\theta) = 0, \\
& \qquad\quad u_{min} \leq u \leq u_{max}, \\
& \qquad\quad x_{min} \leq x \leq x_{max}, \\
& \qquad\quad y_{min} \leq g(x,u,\theta) \leq y_{max}.
\end{aligned}
\tag{121}
$$

In case there was also a secondary criteria, then the optimization was done in two steps. First, the optimal value of the primary objective function is found. In the second step, the primary objective function is contained to its optimal value and the secondary objective function is optimized.

3.2 Steady state optimization

The NLCM toolbox already had the tools to find the steady state of the system and to optimize the steady state (setpoint). In the NLCM implementation, a steady state which satisfies a set of constrains is found with the *lsqnonlin* Matlab function. When the steady state is achieved, the numerical algorithm (Matlab's fmincon or Ipopt) finds the optimum which minimizes (or maximizes) the objective function while satisfying the set of constrains.

We have discovered the optimization task of AWG-DW without reasonable normalization of the internal variables has extremely slow convergence speed. To combat this issue, we changed the units of all the variables which were either too low or high. The air flow rates unit were modified to m^3/h, the refrigerant mass flow rates to $\mathrm{kg\,h}^{-1}$ and the humidities to $\mathrm{g_{water}\,kg^{-1}_{dry\ air}}$. Even though we changed the system to normalize the internal variables and input values into the interval of 1-1000, a proper normalization could improve the performance of numerical algorithms even further.

While building the model of the AWG-DW, the CasADi [25] inside the NLCM creates the derivatives of the constrains and the objective function with respect to the internal variables and inputs.

As a first step, the steady states of AWG-DW were calculated for a six dimensional grid representing the six important variables: external temperature, humidity, the volumetric flow rate in the evaporator and condenser, super-heat temperature in the super-heat controller and the evaporation temperature. This step was done to gain a general understanding of the inner workings of the device and to calculate a reasonable estimate of the optimal values for the following optimization task. In Section 3.3 we describe an interesting phenomenon. When the outside temperature and humidity is low, then the efficiency of AWG-DW (water generation per input power) has two local extremes. This observation makes this step mandatory in our quest to find the global optima rather than just local ones.

In the set point optimization we tested all the implemented algorithms within the *fmincon* Matlab function. The *interior-point* algorithm was both slow and unreliable in converging to the optimum. The *active-set* algorithm achieved the best convergence speed, however, if the initial estimate was not close enough it sometimes did not converge even when we knew the solution exists. In case this happened, the violation of the constrains was often quite high.

Most of the time, the *sqp* algorithm converged to a solution and in case it did not converge, the solution estimate was reasonable (the violation of the set of constrains was reasonably low). However, it was significantly slower than the *active-set* algorithm.

After experimenting with the numerical algorithms, we decided to use a combination of algorithms. The first algorithm was *sqp* and its result was then fed into the *active-set* algorithm as the initial estimate. This way a solution wasss found in all cases when we know it exists and speed of convergence was reasonably fast.

3.3 Results

3.3.1 Water production for given input power

First of all, we decided to investigate the relation between the water production and the total power input of AWG-DW. Such model may be used for water production maximization throughout a day using an economic MPC. We created an optimization task which maximizes the water production for given input power of AWG-DW P_{tot}, constant evaporator air flow rate $120\,\mathrm{m}^3/\mathrm{h}$ and outside temperature and humidity.

Some interesting phenomenon can be observed for low temperature $15\,^\circ\mathrm{C}$ and absolute humidity $5\,\mathrm{g\,kg}^{-1}$. The minimal input power is limited by the minimal compressor rotation speed of $15\,\mathrm{Hz}$ and the minimal refrigerant saturation temperature in the evaporator $0\,^\circ\mathrm{C}$ (to prevent frosting). The electric heater has to be used to achieve minimal refrigerant flow rate (increase the heat transfer in the evaporator).

The water production increases with the input power of AWG-DW, however, the efficiency of water production decreases at first but at $1.25\,\mathrm{kW}$ of input power, the efficiency start increasing once again. This phenomenon is likely caused by the desiccant wheel and it seems to be present only when the temperature and humidity is low.

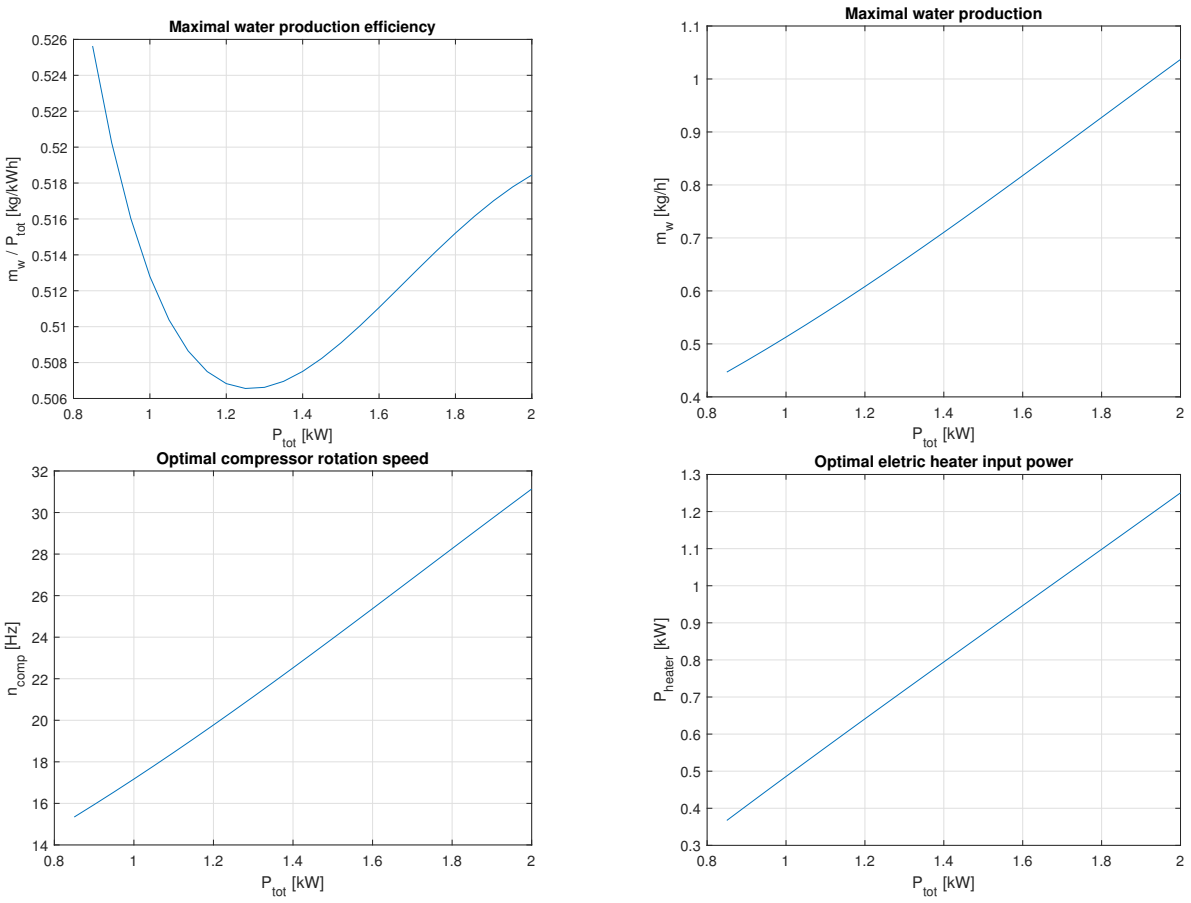

Figure 19: Model optimal setpoints for low temperature $15\,^\circ\mathrm{C}$ and humidity $5\,\mathrm{g\,kg}^{-1}$.

Based on out data analysis, we also investigated the combination of outside temperature $30\,^\circ\mathrm{C}$ and absolute humidity $6.25\,\mathrm{g\,kg}^{-1}$, show in Figs. 20 and 21.

For total input power ($P_{tot} < 0.75\,\mathrm{kW}$), there is not enough power for the compressor and the saturation temperature in the evaporator is above $0\,^\circ\mathrm{C}$. Once the minimal saturation temperature in

the evaporator is reached the maximal efficiency of water production is achieved. After that, the electric heater is turned on, the water production increases until the desiccant upper temperature limit is reached.

At first the air flow rate in the condenser is above the evaporator flow rate to reduce the heat transfer rate in the evaporator. Then it is at its minimal value (flow rate in the evaporator). In this experiment, the condenser air flow rate rises when the maximal desiccant input air temperature is achieved. However, in other experiments Fig. 22, the optimal condenser air flow rate starts increasing to increase the heat transfer and keep the maximal refrigerant saturation temperature within limits.

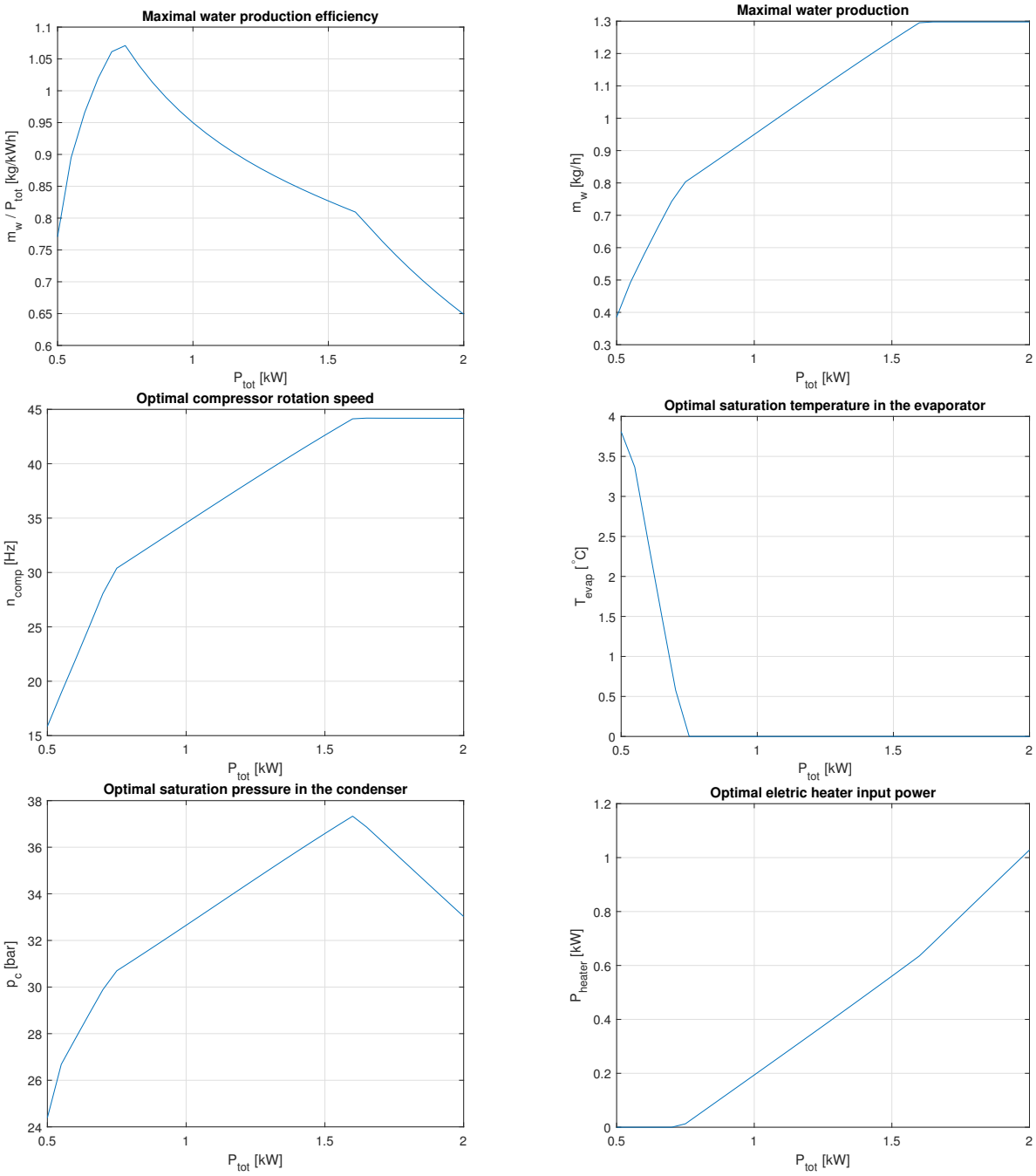

Figure 20: Model optimal setpoints for low temperature $30\,^{\circ}\mathrm{C}$ and humidity $6.25\,\mathrm{g\,kg^{-1}}$.

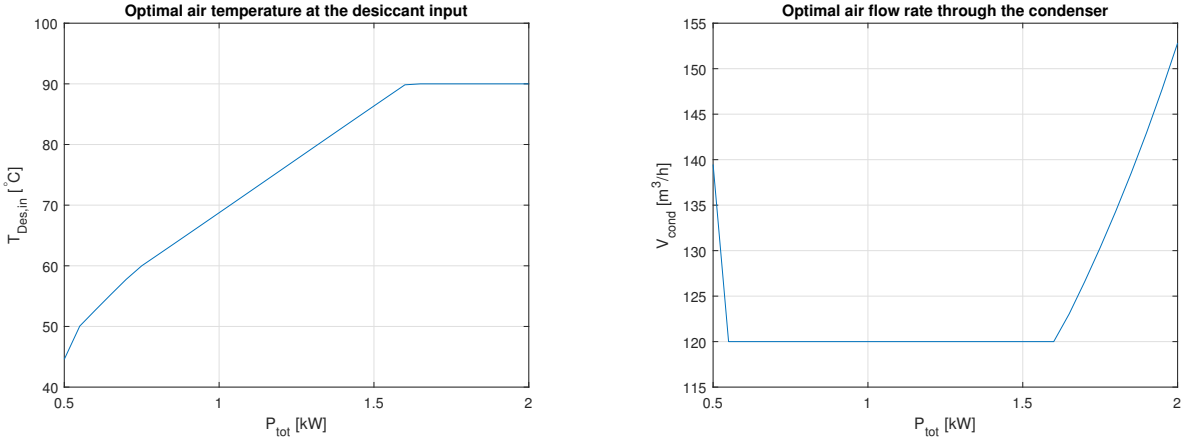

Figure 21: Model optimal setpoints for low temperature $30\,^{\circ}\mathrm{C}$ and humidity $6.25\,\mathrm{g\,kg^{-1}}$.

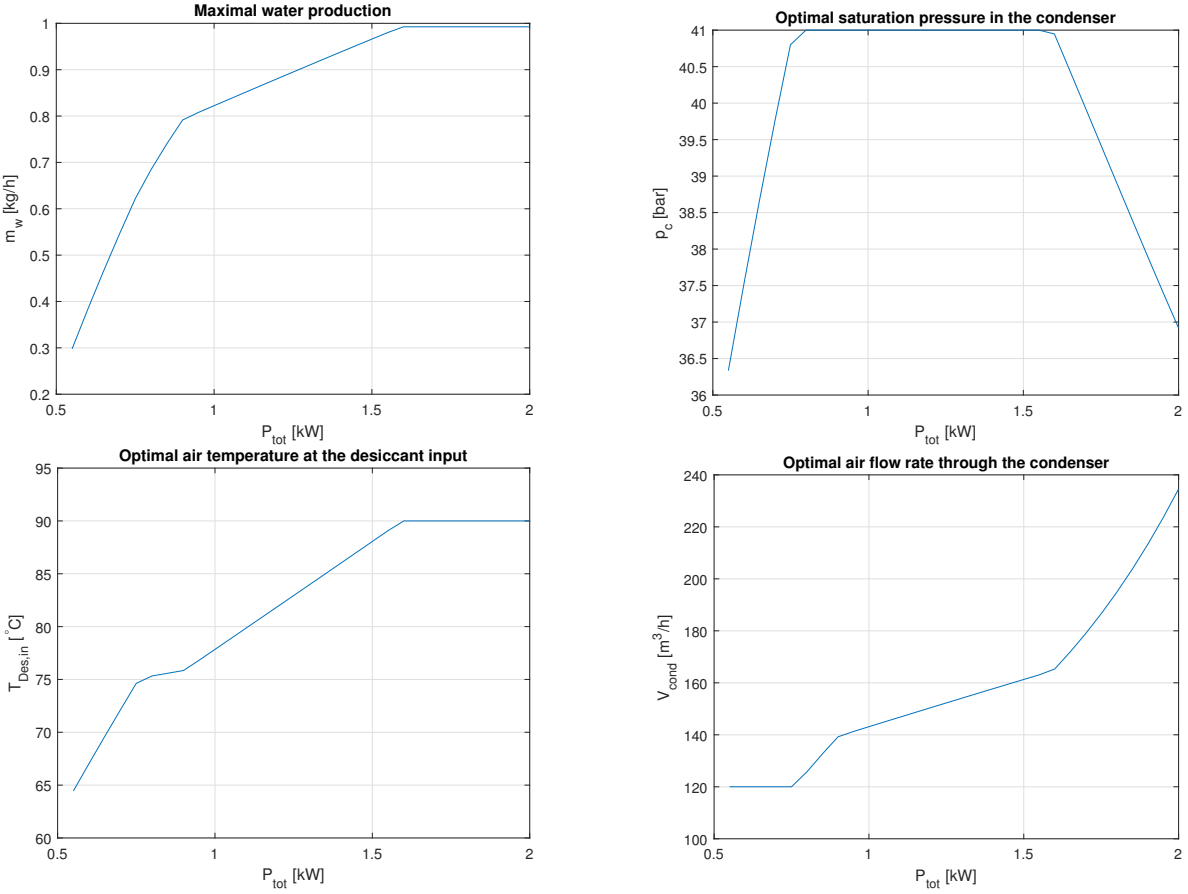

Figure 22: Model optimal setpoints for low temperature $45\,^{\circ}\mathrm{C}$ and humidity $6.25\,\mathrm{g\,kg^{-1}}$.

3.3.2 Maximum water production

In this section, we investigate the condition of maximal water production with constant evaporator air flow rate $120\,\mathrm{m}^3/\mathrm{h}$. The main focus is the usage of the electric heater and the temperature at the desiccant wheel input. At the evaporator input, we want to have low temperature and high absolute humidity of the air. However, an increase in the air temperature at the desiccant wheel input increases the absolute humidity but it increases the output temperature as well.

The results show that the water production is maximized when the desiccant wheel input air temperature is at is upper limit $90\,^\circ\mathrm{C}$ and the saturation temperature in the evaporator is at its lower limit $0\,^\circ\mathrm{C}$. The results of the optimization task are shown in Fig. 23. The amount of generated water is at its maximum when the outside relative humidity is at its maximum (low temperature and high absolute humidity). The dumper valve is opened only to

The compressor rotation speed is way below its maximum rotation speed of $120\,\mathrm{Hz}$ and it was not limited by its operational envelope. However, in the measurements of AWG-DW, the compressor was at the limits of its operational envelope. The plausible explanations for this discrepancy have already been discussed in this thesis.

The model results also suggest the water production could be increased by increasing the air flow rate through the evaporator. As we have already mentioned, the measured data mostly had the same evaporator air flow rate, therefore there is a lot of uncertainty in this regard.

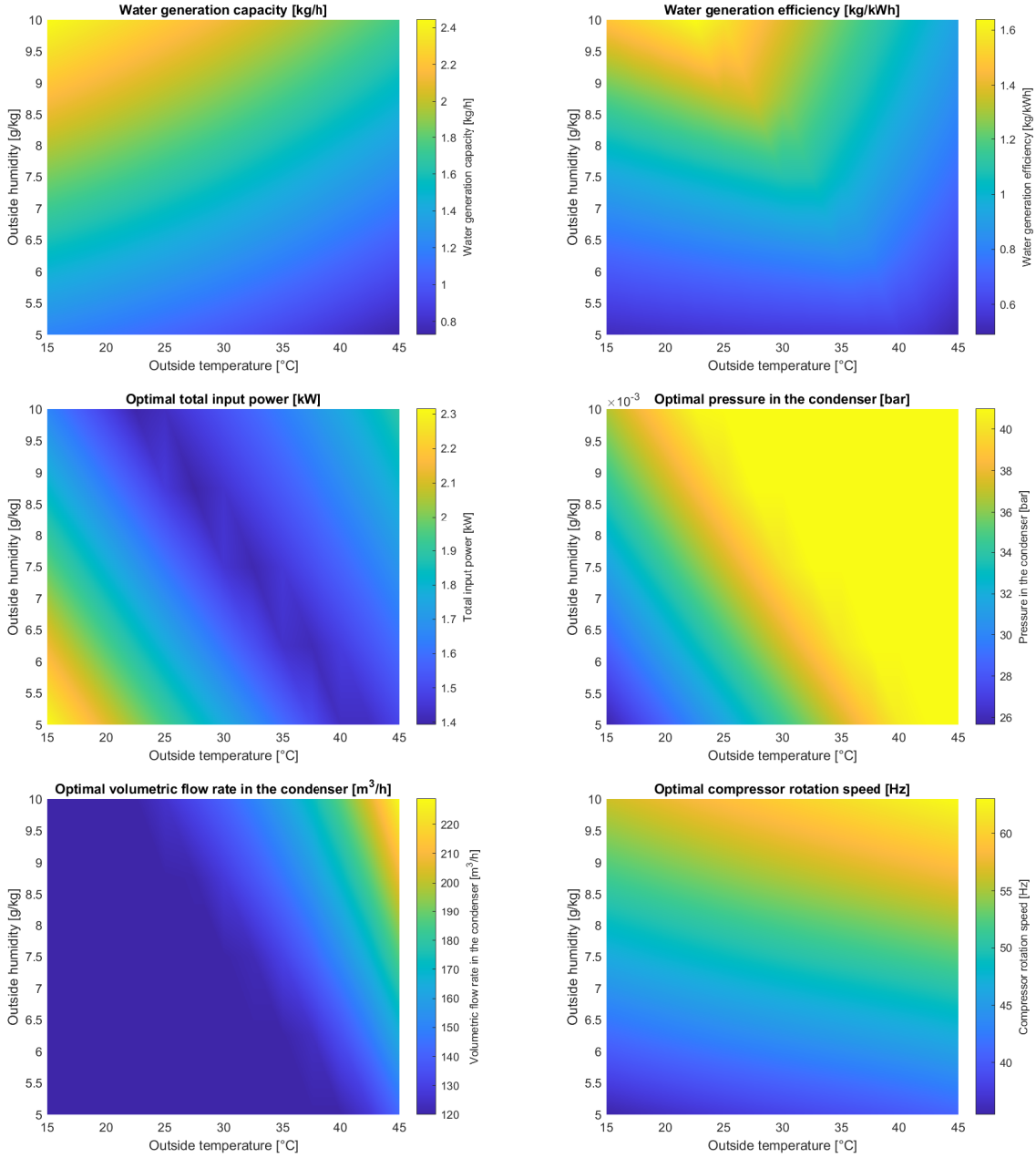

Figure 23: Model optimal setpoints for maximal water production

3.3.3 Maximum water production efficiency

In case the device is running from a limited power source, for example batteries, maximum efficiency of water production is desirable. We created an optimization task to maximize water production efficiency (production per input power) with constant evaporator air flow rate $120\,\mathrm{m}^3/\mathrm{h}$.

We are interested mainly in the electric heater usage. The measurements (Apendix A) suggests that for certain outside conditions the heater should be used to a certain extent to maximize the efficiency of water production. However, the results did not show such phenomenon. According to the model, the heater should be used only for low temperature and low humidity conditions to achieve the minimal compressor rotation speed, otherwise it should be turned off to achieve maximal efficiency.

Interestingly, if the outside temperature and absolute humidity is high, the saturation temperature in the evaporator should get above $0\,^\circ\mathrm{C}$ to achieve the maximum efficiency. This happens only when saturation temperature in the condenser is reached. The increase in this saturation temperature reduces the amount of water production, but it also reduces the compressor input power and keep the desiccant wheel input air temperature high. When the dumper valve opens to allow higher flow rate through the condenser and reduces the output air temperature.

Another interesting thing to note is that water generation capacity seems to correlate with boundary where the condenser refrigerant pressure reaches its upper limit. This is most likely caused by the dumping of heated air in the dumper air valve. The model results also suggest an increase the air flow rate through the evaporator should improve the the water production efficiency. As we have already mentioned, the measured data mostly had the same evaporator air flow rate, therefore there is a lot of uncertainty in this regard.

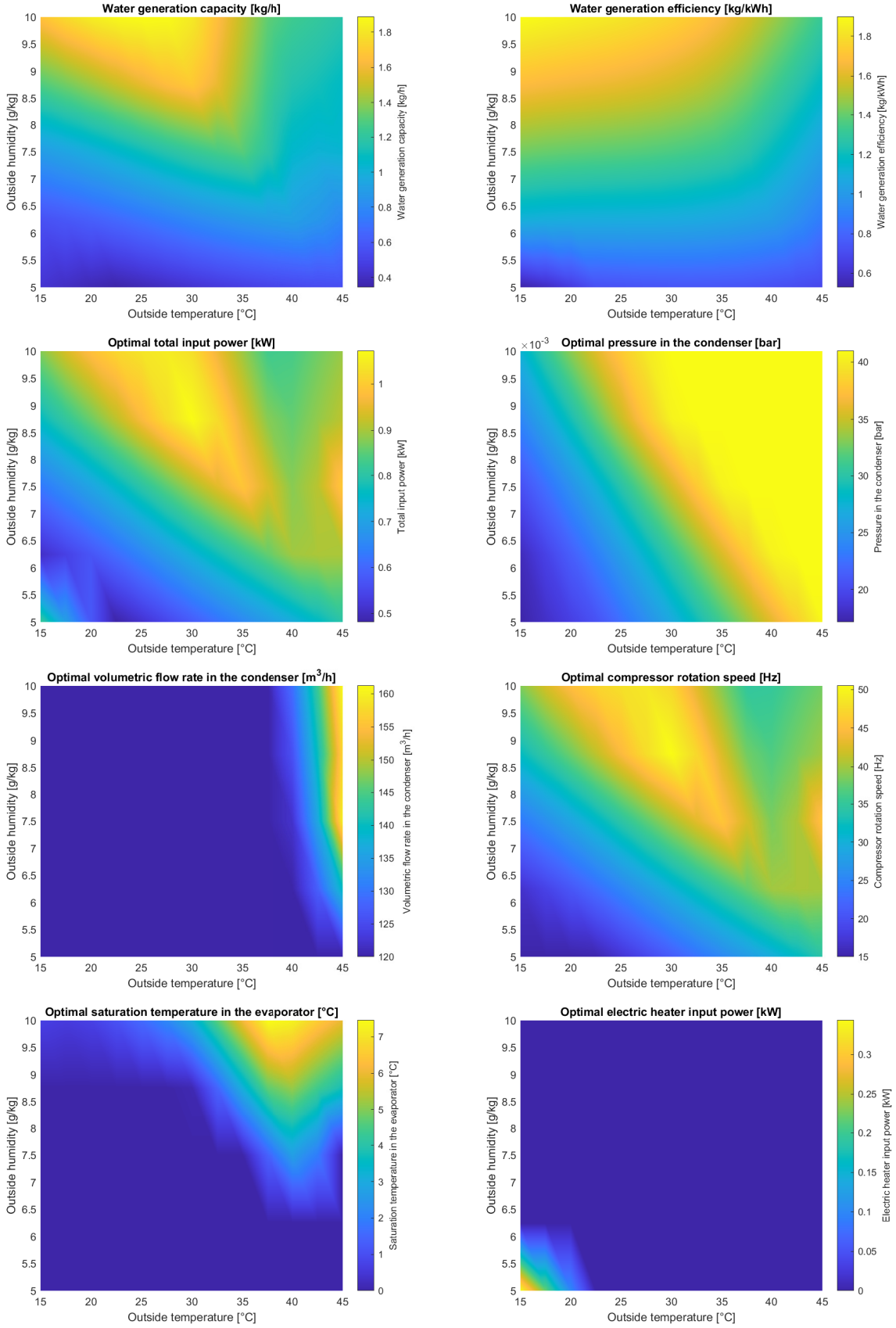

Figure 24: Model optimal setpoints for the maximal water production efficiency

Chapter 4
Conclusion

In this thesis, the topic of air-water-generators (AWG) was investigated. The main focus was one of such units we called AWG-DW. We described the basic operation principles of this AWG device and then split it into its components. The individual components were modeled and calibrated to the measured data. We debated the possibility of water condensation in the heat recovery unit, however, there exists no measurement of the absolute humidity change within the recuperator. Other inconsistencies in the measurements were identified. Mainly a defective heat balance in the refrigerant cycle, which was most likely caused by insufficient refrigerant charge, and improper mounting of the temperature sensor.

Nevertheless, the components models were put together to create the model of AWG-DW. Despite the defective measurements, the overall water production of the model is comparable to the measurements, but to derive meaningful results a new set of measurements has to be done (currently in preparation).

We first investigated the relationship between water generation and input power. An optimization task was created, which maximizes the water production for given input power and outside air conditions. This relationship will serve as the main input for daily production maximization in an economic MPC. We observed various limitations which manifest in the results of the task. For low input power, the saturation temperature in the evaporator is above $0\,^{\circ}\mathrm{C}$ because there is not enough power for the compressor. Once the compressor is working at its maximum, the electric heater is turned on. If the maximum saturation temperature in the condenser is reached then the dumper valve starts to open. The device then reaches its maximum reasonable input power when the upper temperature limit of the desiccant wheel is reached. The device is capable of using more power, however, the water production does not change and the extra energy is wasted through the air dumper valve.

After that, we focused on the two main scenarios of operation: when the electricity is abundant and the water production is maximized, and when the electricity is scarce (battery power) and therefore maximum efficiency is prioritized. An optimization task was created for both scenarios.

If we desire the maximum water production, the electric heater should be used to reach the upper temperature limit of the desiccant wheel. The saturation temperature in the evaporator is at its lower temperature limit $0\,^{\circ}\mathrm{C}$ to prevent frosting. The air dumper valve should be opened only to keep the saturation pressure in the condenser below its maximum. The maximum water production is achieved when the outside air has maximal relative humidity i.e. the temperature is low and absolute humidity is high.

If we desire the maximum water production efficiency i.e. maximum production per unit of input power, then the electric heater should not be used unless it is needed to reach the minimum rotation speed of the compressor (low outside temperature and humidity). The temperature of the evaporator is often at its lower limit. However, for high outside air temperature and humidity, the maximum efficiency is achieved with saturation temperatures in the evaporator above the lower limit. The dumper valve should only be used to keep the saturation temperature in the condenser below its upper limit.

4.1 Future work

The next logical step in modeling AWG-DW is to resolve the data inconsistencies, most likely caused by either improper or non-existent measurements. The refrigerant flow rate should be measured by a dedicated sensor. The dataset should be also extended to include measurements for a different evaporator air flow rate. The results of this thesis will also form the basis of the upcoming economic model predictive controlled to maximize production throughout the day. The model has proven itself to be a valuable tool in diagnosing system behavior and in fault detection and it can be also utilized to estimate the effects of component changes. Lastly, we would like to implement proper normalization into the steady state optimization routines of the NLCM toolbox.

References

[1] R. Tu and Y. Hwang, "Reviews of atmospheric water harvesting technologies," *Energy*, vol. 201, p. 117630, 2020.

[2] H. Jarimi, R. Powell, and S. Riffat, "Review of sustainable methods for atmospheric water harvesting," *International Journal of Low-Carbon Technologies*, vol. 15, no. 2, pp. 253–276, 2020.

[3] N. Pokorny, V. Shemelin, and J. Novotny, "Experimental study and performance analysis of a mobile autonomous atmospheric water generator designed for arid climatic conditions," *Energy*, vol. 250, p. 123813, 2022.

[4] N. Pokorný, T. Matuška, and V. Shemelin, "Compact device for obtaining water from the air," Patent, Jan, 2021. [Online]. Available: https://isdv.upv.cz/doc/FullFiles/Patents/FullDocuments/308/308655.pdf

[5] X. Kong, Y. Zhang, and J. Nie, "A new mixture refrigerant for space heating air source heat pump: Theoretical modelling and performance analysis," *Applied Sciences*, vol. 8, no. 4, p. 622, 2018.

[6] *Non-Linear Continuous state space Models*. Prague: Honeywell Prague Laboratory, 2017.

[7] *Vapor Compression Cycle toolbox*. Prague: Honeywell Prague Laboratory, 2015.

[8] E. W. Lemmon, I. H. Bell, M. L. Huber, and M. O. McLinden, "NIST Standard Reference Database 23: Reference Fluid Thermodynamic and Transport Properties-REFPROP, Version 10.0, National Institute of Standards and Technology," 2018. [Online]. Available: https://www.nist.gov/srd/refprop

[9] I. H. Bell, J. Wronski, S. Quoilin, and V. Lemort, "Pure and pseudo-pure fluid thermophysical property evaluation and the open-source thermophysical property library coolprop," *Industrial & Engineering Chemistry Research*, vol. 53, no. 6, pp. 2498–2508, 2014. [Online]. Available: http://pubs.acs.org/doi/abs/10.1021/ie4033999

[10] W. Pirompugd and S. Wongwises, "Actual dry-bulb temperature and equivalent dry-bulb temperature methods for wavy fin-and-tube heat exchangers with dehumidification," *International Journal of Heat and Mass Transfer*, vol. 106, pp. 675–685, 2017.

[11] G. Zhang, B. Wang, X. Li, W. Shi, and Y. Cao, "Review of experimentation and modeling of heat and mass transfer performance of fin-and-tube heat exchangers with dehumidification," *Applied Thermal Engineering*, vol. 146, pp. 701–717, 2019.

[12] J. L. Threlkeld, *Thermal environmental engineering*. Prentice Hall, 1970, vol. 11.

[13] J. Wang and E. Hihara, "Prediction of air coil performance under partially wet and totally wet cooling conditions using equivalent dry-bulb temperature method," *International Journal of Refrigeration*, vol. 26, no. 3, pp. 293–301, 2003.

[14] L. Rosario and M. M. Rahman, "Analysis of heat transfer in a partially wet radial fin assembly during dehumidification," *International journal of heat and fluid flow*, vol. 20, no. 6, pp. 642–648, 1999.

[15] L. Erickson, "Rating equations for positive displacement compressors with auxiliary suction ports," 1998.

[16] E. W. Weisstein, "Cubic formula," *https://mathworld. wolfram. com/*, 2002.

[17] J. Čermák, *Ventilátory*, 1st ed. Praha: Nakladatelství technické literatury, 1974.

[18] Z. Du and X. Lin, "Research progress of rotary desiccant wheel optimization technology," in *IOP Conference Series: Earth and Environmental Science*, vol. 512, no. 1. IOP Publishing, 2020, p. 012181.

[19] T. Ge, Y. Li, R. Wang, and Y. Dai, "A review of the mathematical models for predicting rotary desiccant wheel," *Renewable and Sustainable Energy Reviews*, vol. 12, no. 6, pp. 1485–1528, 2008.

[20] A. A. Pesaran and A. F. Mills, "Moisture transport in silica gel packed beds—i. theoretical study," *International Journal of Heat and Mass Transfer*, vol. 30, no. 6, pp. 1037–1049, 1987.

[21] D. Charoensupaya and W. M. Worek, "Parametric study of an open-cycle adiabatic, solid, desiccant cooling system," *Energy*, vol. 13, no. 9, pp. 739–747, 1988.

[22] C. Jia, Y. Dai, J. Wu, and R. Wang, "Use of compound desiccant to develop high performance desiccant cooling system," *International journal of refrigeration*, vol. 30, no. 2, pp. 345–353, 2007.

[23] H. Kang, G. Lee, and D.-Y. Lee, "Explicit analytic solution for heat and mass transfer in a desiccant wheel using a simplified model," *Energy*, vol. 93, pp. 2559–2567, 2015.

[24] D.-Y. Lee and D.-S. Kim, "Analytical modeling of a desiccant wheel," *International journal of refrigeration*, vol. 42, pp. 97–111, 2014.

[25] J. A. E. Andersson, J. Gillis, G. Horn, J. B. Rawlings, and M. Diehl, "CasADi – A software framework for nonlinear optimization and optimal control," *Mathematical Programming Computation*, vol. 11, no. 1, pp. 1–36, 2019.

[26] F. Wahl and T. Espinasse, "Multivariable parametric regression under shape constraints," 2018.

[27] ——, "Simplex regression: Multivariable parametric regression under shape constraints," 2018.

Appendix A
AWG-DW experiment data 2021

As we have already discussed in the thesis, we have identified some inconsistencies in the measured data. The refrigerant temperature at condenser input $T_{r,c,i}$ is probably incorrectly measured and the temperature at the condenser output should be a temperature of sub-cooled liquid, however, the refrigerant is likely still in a mixed phase.

	$X_{a,c,i}$ [g/kg]	$X_{a,e,i}$ [g/kg]	$X_{a,e,o}$ [g/kg]	$\dot{V}_{a,e}$ [m^3/h]	P_{comp} [kW]	f_{comp} [Hz]	p_{valve} [%]	P_{heater} [kW]	$\dot{m}_w$ [kg/h]	P_{tot} [kW]	$\dot{m}_w/P_{tot}$ [kg/kWh]
Exp 1	5	13.3	5.88	120	0.73	79.2	0	1.52	0.91	2.82	0.322
Exp 2	7.5	16.4	6.41	120	1.28	103	0	0.865	1.23	2.61	0.471
Exp 3	10	19.1	7.38	120	1.29	105	31.1	1.05	1.45	2.96	0.489
Exp 4	5	13.2	7.23	120	1.26	99.9	25.8	0.767	0.75	2.31	0.325
Exp 5	7.5	15.8	7.68	120	1.27	105	40.8	1.05	1	2.65	0.377
Exp 6	10	17.1	7.26	120	1.29	105	38.7	0.9	1.25	2.62	0.477
Exp 7	5	12	7.83	119	1.24	102	44.9	0.758	0.55	2.53	0.217
Exp 8	7.5	15.2	8.29	115	1.25	106	68.1	1.18	0.807	2.87	0.281
Exp 9	10	16.8	7.95	97.3	1.25	107	86.8	1.1	0.953	2.71	0.352
Exp 10	5	5.76	4.62	113	0.125	19.2	0	0	0.229	0.41	0.559
Exp 11	7.5	7.9	5.12	120	0.088	31.3	0	0	0.483	0.406	1.19
Exp 12	7.5	8.33	4.77	120	0.073	40.4	0	0	0.577	0.575	1
Exp 13	10	14.4	6.45	120	1.13	98	0	0	1.18	1.46	0.81
Exp 14	5	9.06	5.77	120	0.57	74.3	0.549	0	0.383	0.888	0.431
Exp 15	7.5	12.2	6.38	120	1.2	99.2	4.92	0	0.9	1.48	0.608
Exp 16	10	13.6	6.65	120	1.2	103	31	0	0.99	1.51	0.655
Exp 17	5	9.23	6.51	120	1.2	103	42.5	0	0.333	1.53	0.218
Exp 18	7.5	10.9	7.2	120	1.19	107	58.2	0	0.513	1.6	0.321
Exp 19	10	12.8	7.25	115	1.2	107	60.5	0	0.821	1.66	0.495
Exp 20	10	15.1	7.08	120	1.22	106	36	0.35	1.33	1.99	0.668
Exp 21	7.5	12.1	7.3	120	1.2	106	47	0.35	0.78	1.97	0.396
Exp 22	10	14.5	8.05	120	1.22	105	54.8	0.456	0.922	2.11	0.436

Table 9: Mean steady-state measurements in AWG-DW

	$T_{a,c,i}$ [°C]	$T_{a,c,o}$ [°C]	$T_{a,d,i}$ [°C]	$T_{a,d,o}$ [°C]	$T_{a,e,i}$ [°C]	$T_{a,e,o}$ [°C]	$T_{a,r2,o}$ [°C]	$T_{r,c,i}$ [°C]	$T_{r,cond}$ [°C]	$T_{r,c,o}$ [°C]	$T_{r,e,i}$ [°C]	$T_{r,evap}$ [°C]	$T_{r,e,o}$ [°C]
Exp 1	15.3	52	89.2	48.4	20	6.72	39	65.7	45.6	40.3	2.47	2.47	10.5
Exp 2	16.5	68.3	89.5	45.9	23	8.09	38.3	81.5	56	49.7	2.25	2.25	10.2
Exp 3	21.2	64.8	90.3	46.2	25.4	10.2	39.4	82.8	54.6	49.4	3.34	3.34	11.3
Exp 4	26.1	70.9	89.6	51.1	22.3	10.4	42.6	85.7	58	54.1	2.19	2.19	10.2
Exp 5	26.6	63.5	89.2	48.5	24.1	11.2	41.6	81.7	54.5	50.7	3.03	3.03	11
Exp 6	25.5	62.8	84.6	46.5	24.2	10.1	39.4	81.3	54.1	49.1	2.76	2.76	10.8
Exp 7	35.5	65.9	84.4	57.8	23	11.6	48	84.7	56.8	53.7	2.07	2.07	10.1
Exp 8	36.3	59.4	89.2	55.8	25.3	12.5	47.5	83	53.9	50.9	2.55	2.55	10.6
Exp 9	35.4	57.8	90.6	50.5	24.9	12.2	43.1	82.6	53	49.9	1.55	1.55	9.55
Exp 10	13.9	23.7	23.7	20.3	8.66	3.96	17.8	35.7	24	21.3	0.839	0.839	8.84
Exp 11	15.1	31.3	31.3	23.1	11.8	4.85	19.8	42.1	31.2	27.5	1.56	1.56	9.56
Exp 12	15.2	34.2	34.2	23.5	12.6	4.2	20.3	46.5	33.2	28.8	0.899	0.899	8.9
Exp 13	19.4	65.3	65.3	34.7	20.5	8.16	29.7	77.7	54.3	48.2	2.06	2.06	10.1
Exp 14	24.8	55.4	55.4	37	16.5	6.84	31.4	69.2	48.3	43.3	0.772	0.772	8.77
Exp 15	24.9	71.7	71.7	42.4	19.5	8.27	35.1	83.7	58.3	53.1	1.31	1.31	9.31
Exp 16	25.5	65.3	65.3	39.7	20.7	8.86	33.7	79.9	55.5	50.5	1.36	1.36	9.36
Exp 17	35.7	64.2	64.2	49.6	20.7	9.12	42.2	81.1	56	52.5	-0.158	-0.158	7.84
Exp 18	35.4	58	58	45.5	20.9	10.3	39.2	76.6	52.8	49.6	1.15	1.15	9.15
Exp 19	35.2	57.8	57.8	44.9	21.1	10.5	38.3	77.6	53.1	49.7	1.31	1.31	9.31
Exp 20	25.4	62.3	70.7	42.7	22.3	9.78	35.8	77.4	53.9	49	2.46	2.46	10.5
Exp 21	34	60.7	69.2	49.5	20.9	10.4	41	77.8	53.7	49.8	1.64	1.64	9.64
Exp 22	35.7	60.3	71.3	51.4	23.4	11.8	42.7	80.4	54.3	50.9	2.96	2.96	11

Table 10: Mean steady-state temperatures measured in AWG-DW